



INTELLIGENT FIBER OPTIC SYSTEMS

650 Vaqueros Ave., Sunnyvale, CA 94085

Phone: (408) 328-8610 Fax: (408) 328-8614

PI: Dr. Behzad Moslehi

bm@ifos.com

Ultra-High-Speed Photonic Add-Drop Multiplexers For Wave-Division-Multiplexed Networking

DOE SBIR Phase II Final Report

Reporting Period: June 15, 1999 – June 14, 2002

Grant No.: DE-FG03-98ER82599

Project Period: June 15, 1999 – June 15, 2002

Dr. George Seweryniak, ER-31

19901 Germantown Road

Germantown, Maryland 20874-1290

Phone: (301) 903-0071

sewerynia@er.doe.gov

TABLE OF CONTENTS

Abbreviations and Acronyms	3
Chapter 1 Introduction	5
Chapter 2 Network Modeling and Analysis	6
2.1 Advantages of WADM	6
2.2 Analysis and Application	6
2.3 Reconfigurable WADM Network Connectivity	7
2.4 Network Survivability	8
2.5 Grooming Optical Networks	11
Chapter 3 WADM Design and Simulation	23
3.1 WADM Overview	23
3.2 Optimized Device Simulation and Design	26
3.3 Device Design	31
3.4 Selecting the Refractive Index of the Polymer	33
3.5 SPF with Polymer Overlay Power Distribution	35
3.6 Sensitivity of Power Distribution to the Device Parameters	40
Chapter 4 Test Methodologies	43
4.1 Optical Tests: Static and Dynamic Devices	43
4.2 Preparation for Network Insertion Test	44
Chapter 5 Commercialization	47
5.1 Market Potential	47
5.2 Market Value	47
5.3 WADM Applications	50
5.4 Commercial Expansion	52
Chapter 6 Conclusion	53
Chapter 7 References	54

Abbreviations and Acronyms

Term	Definition
AC	Alternating current
ASE	Amplified spontaneous emission
AWG	Arrayed waveguide grating
ADM	Add-drop multiplexer
BER	Bit error rate
BLSR	Bidirectional line switched ring
BP	BEM propagation method
BPW	Parallel wavelength
DC	Direct current
DCD	Dispersion compensating device
DGD	Differential group delay
DCS	Digital crossconnect systems
DWDM	Dense wavelength division multiplexing
EO	Electrical-to-Optical
EDFA	Erbium doped fiber amplifier
FBG	Fiber Bragg grating
FR	Final Report
IFOS	Intelligent Fiber Optic Systems
ICFG	Intra-core fiber grating
ILP	Integer linear programming
IO	Input Output
ITU	International Telecommunications Union
LAN	Local area network
OCH DPRING	Optical Channel Dedicated Protection Ring
OE	Optical to electrical
OEO	Optical to electrical to optical
OFA	Optical fiber amplifier
ONE	Optical network elements
OTDR	Optical time domain reflectrometers
OTN	Optical transport network
POI	Power overlap integral
PI	Principal Investigator

PMD	Polarization mode dispersion
SNC	Subnetwork connection
SONET	Synchronous optical network, ANSI Standard
SPF	Side polished fibers
SL	Span loss
SPRING	Shared protection rings
SRF	Side removed fiber
TDM	Time division multiplex
TR	Transmit Receive
UPSR	Unidirectional path switched ring
WADM	Wavelength add-drop multiplexer
WDM	Wavelength division multiplexing

Chapter 1 Introduction

This report presents the final summary of activities and results of the DOE SBIR Phase II project, *Ultra High Speed Photonic Add-Drop Multiplexers for Wave Division Multiplexed Networking*. The objective of this program was to analyze, model, design and implement ultra-high speed photonic Dense Wavelength Division Multiplexing (DWDM) networks using Wavelength Add-Drop Multiplexers (WADMs).

The report is divided into five sections: network modeling and analysis; WADM design and simulation; test methodologies; commercialization; the conclusion.

Chapter 2 starts with definitions and advantages of different classes of WADMs. In this Chapter, the main issues of reconfigurable DWDM network connectivity and the traffic-grooming problems for WDM/SONET ring network are described and a brief overview of current standards is presented. The optical network survivability and optical ring configurations have many applications in ultra high speed photonic networks. The design and analysis of efficient optical networks are based on both network configuration and traffic grooming. In this project both optical ring and optical mesh topologies were examined and different ring interconnection strategies were considered. A new algorithm for traffic grooming is developed and the numerical results for single-hop, multi-hop and interconnecting double-ring and multi ring cases are reported.

Chapter 3 reports the WADM design and simulation results. The modeling approaches, and the device simulation model and the design parameters are described. After a brief introduction of the Side Removed Fiber model, basic design rules for a device with Intra-Core Fiber Grating with Active Optical Polymer are introduced.

The highlights of the device design, simulation results, refractive index analysis, and sensitivity of power distribution to the device parameters are all included in Chapter 3. The results of the effect of remaining cladding thickness variation and effect of polymer thickness and refractive index variation are also presented in Chapter 3.

Chapter 4 describes the test methodologies developed for static and dynamic WADM modules testing and additional and final production verification for the next phase of this project. Preparation efforts required for network insertion testing and network test plans for evaluation of both static and dynamic WADMs for different applications in communications network, cluster computing networks and sensor networks are also included.

Chapter 5 covers the commercialization plan for IFOS's WADM modules: market potential of WADM; WADM applications; commercial expansion.

Chapter 6 discusses the results of this project.

Chapter 2 Network Modeling and Analysis

This section covers the development of new models for the analysis and application of static and reconfigurable wavelength add-drop multiplexers (WADMs) in optical networks.

Currently, the wavelength division multiplexer (WDM) simultaneously transmits data on multiple carrier wavelengths over one fiber. With this capability, WDM provides a solution to expand the capacity of existing fiber. WDM is often more cost effective than other solutions, such as adding fiber or replacing the current TDM transport system with higher rate system. To expand this capability and reduce the network cost, IFOS proposes the wavelength add-drop multiplexer (WADM).

2.1 Advantages of WADM

A significant advantage of WADM is cost reduction. Currently, the SONET ring is often used in optical networks. The SONET ring supports system reliability as it typically recovers from a failure within 100 ms. For this stability; some network carriers use the ring topology to build networks. For example, Figure 1 shows the nationwide Sprint SONET ring networks that consist of interconnected rings

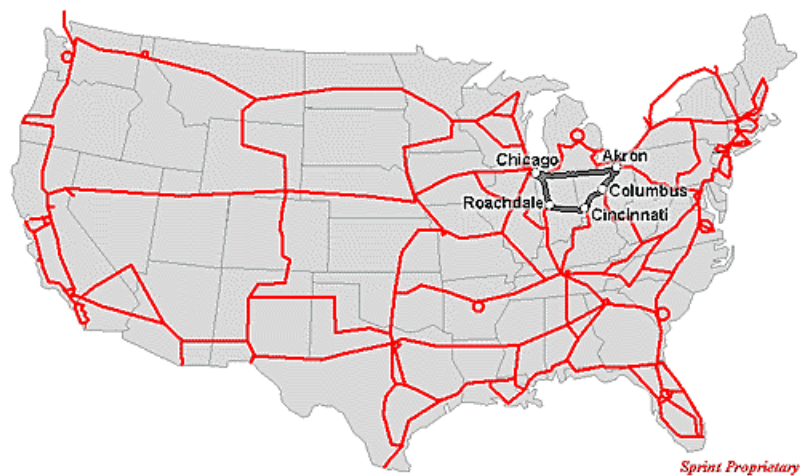


Figure 1 Sprint Nationwide Backbone Fiber Network of Interconnected Rings

A weakness of the WDM/SONET ring is the cost of required electronic equipment, the add-drop multiplexer. Currently, the cost of a SONET ADM that supports OC-48 (2.488 Gbps) is approximately \$100,000 each. However, the WADM can be fabricated for less than one \$1000 each. For network performance, WADM increases the transparency of the network, but the cost of the WADM virtually does not increase when the line speed is boosted. The best utilization of WADMs is on selected nodes and wavelengths where traffic does not need to be added and dropped.

In point-to-point deployment, WDM technology only expands the capacity of physical links between the adjacent nodes on the ring. Every wavelength is electronically terminated at every node, whether or not a wavelength carries traffic that is sourced from or sunked to at that node. Terminating every wavelength at every node greatly increases the required SONET terminal equipment: ADMs. WADMs provide the advantage of optical networking in which a wavelength optically bypasses a node, reducing the network cost. Form maximum savings, network planning is necessary: assign traffic to appropriate wavelengths. This network planning issue is referred to as *traffic grooming problem*, also known as *NP-complete* for general traffic.

2.2 Analysis and Application

This section covers the Phase II development of new models for the analysis and application of static, dynamic, multiple, and reconfigurable WADMs in optical network. Single-ring architectures employing

WADM, networks of interconnected rings, optical network architectures, and network survivability with ring topology are discussed.

For this task of Phase II, WADMs were analyzed in two forms of optical local area network (LAN) architecture:

Single-hop: nodes, end users, communicate with one another directly, without assistance from an intermediate node

Multi-hop: information, when flowing from a source to the destination, may need to be processed, stored and forwarded, by one or more intermediate nodes.

2.2.1 Static WADM

Static WADMs are unable to directly connect two arbitrary nodes in a network. However, the connection from the source node to the destination node may need to traverse through intermediate nodes. In this case, static WADMs are practical and economical solutions for multi-hop networks.

When nodes employ static WADMs with fixed wavelength-tuning patterns, a multi-hop network architecture is appropriate. To achieve the optical network communications system objective of minimum cost, minimum packet delay, maximum input, etc., requires determining the static WADM configuration at each node for a given pattern of traffic flow.

2.2.2 Dynamic WADM

When nodes employ dynamic WADMs with wavelength agility/tunability, a single-hop network architecture is appropriate: dynamic WADMs provide the agility that single-hop networks require. Dynamic WADMs can establish a direct connection that is needed in single-hop networks. Single-hop networks incorporate more intelligence, and require more complex signaling and protocols.

2.2.3 Multiple WADM

A node with a large amount of traffic may require multiple WADMs. The total number of WADMs in a network may dominate the network cost. However, instead of minimizing the number of wavelengths, an important alternative is minimizing the total number of WADMs used in the network.

2.3 Reconfigurable WADM Network Connectivity

This section describes the issues of reconfigurable DWDM network connectivity.

WADM network connectivity is the capability of providing standardized optical level interface connections between dissimilar Optical Network Elements (ONEs), possibly from multiple suppliers, and minimizing the need for gateway functions. Gateway functions include those typically provided by equipment that performs electrical-to-optical (EO) and/or optical-to-electrical (OE) conversions associated with a ONE optical interface that allow compatible internetworking. WADM network connectivity can allow the following capabilities:

- Interconnection of different DWDM sub-networks at the optical level with reduced need for EO and OE conversion functions
- Simplified designs of transport networks
- Optical level interconnections between service providers (network node interface) and customers (user network interface) to enhance service offerings with many compatible operations, administration and maintenance functions supported between ONEs from different suppliers

Developing dynamically reconfigurable optical networks will allow allocating bandwidth faster at an economical cost. The goals for network connectivity of DWDM systems are described in detail in Telcordia document GR-2918-CORE [1], and in the latest Optical Transport Network (OTN) industry standards recommendations G.692 [2] and G.959.1 [3].

The OTN industry standards for wavelength assignments and power density of the DWDM client signal inputs are not yet established for WADM network connectivity goals. In Telcordia GR-1312-CORE [4] the specifics of *proprietary* DWDM systems are described, but standardization is not yet developed. In this case, it is expected that early DWDM implementations will require transponders. Using transponders that incorporate standardized client tributary input output (IO) signals will allow client signals to interconnect from any vendor unit that complies with a number of different client interface standards.

Today, with optical to electrical conversion, the standardized client signal can be processed in the electrical domain. Conversion back to the optical domain, prior to being combined with other client signals of the same or different type, can be precisely controlled *prior* to the optical multiplexing. This level of control is necessary to maintain the optical power levels and the linearity of client signals such that nonlinear optical degradations, such as Stimulated Brillouin Scattering (SBS), Four Wave Mixing (FWM), etc., do not occur as the client signals are combined into a single composite signal.

The DWDM side remains proprietary; the tributary points of interconnection are standardized. There are currently two broad categories of DWDM systems, *Transverse Compatible* and *Proprietary/Opaque*.

- Transverse Compatible systems are readily extensible to the envisioned optical transport network.
- Proprietary/Opaque systems must adapt client signals, typically in the electrical domain with transponders, before combining them on the multi-wavelength supporting fiber. This is proprietary as client signal adaptation and wavelength selection are not based on standards. In current standards (G.709 [5], G.798 [6] and G.959.1 [3]) governing transverse compatibility requirements, 3R (Reamplification, Reshaping, Retiming) regeneration functions involving optical-to-electrical-to-optical (OEO) processing and/or wavelength conversion, but not transponders, continue to be necessary across these transverse compatible optical interfaces.

Due to the industry standards agreements to forgo optical transparency across the client interface by using a *digital wrapper* to encapsulate client signals, OEO processing with some level of regeneration, 1R, 2R or 3R, will be required. The past two years, further work has been completed in the OTN industry standardization efforts to progress towards these transverse compatibility goals.

2.4 Network Survivability

As discussed in the Phase II project proposal, the key questions for Phase II work include how to develop protection mechanisms that overcome failure events such as fiber cuts, node failures, etc.

Rerouting traffic in the optical domain, using linear, ring or mesh architectures, is an important issue in industry; it must be comparable with existing protection approaches such as those used in SONET self-healing rings. This section covers Optical Ring Configurations, OCH DPRING Function, and Protection in Multi-ring Optical Networks.

2.4.1 Optical Ring Configurations

The most complex network architecture is a ring add-drop configuration that provides enhanced add-drop functionality and reliability. This configuration offers a multitude of traffic grooming capabilities that require attentive administration to ensure efficient bandwidth management, performance monitoring, and network protection. Ring configurations are also the most reliable form of network protection, as there are two paths to any element in the ring. If one path is cut or equipment along a particular path malfunctions, traffic is diverted or switched to the other operational path. Adding WADM elements will enable add-drop capabilities at every point in the ring.

Optical layer protection mechanisms protect physical layer transmission from defects with a single management layer. These protection switching mechanisms may be based on the optical channel or the optical multiplex section layer. Several types of protection switching mechanisms are available at the optical layer. These mechanisms can be categorized into the following six configurations:

- Optical Channel Dedicated Protection Ring (OCH DPRING)

- Two-Fiber Optical Multiplex Section Shared Protection Ring (2F OMS SPRING)
- Two-Fiber Optical Channel Shared Protection Ring (2F OCH SPRING)
- Four-Fiber Optical Multiplex Section Shared Protection Ring
- Without Span Protection (4F OMS SPRING)
- Four-Fiber Optical Multiplex Section Shared Protection Ring With Span Protection (4F OMS SPRING/SP)
- Four-Fiber Optical Channel Shared Protection Ring With Span Protection (4F OCH SPRING/SP)

The OCH DPRING is similar to the SONET unidirectional path switched ring (UPSR) which is always a two-fiber ring. This type of ring is useful when most point-to-point connections are to a few hubs. When the point-to-point connections are mesh-like, the optical counterparts to the SONET bi-directional line-switched ring (BLSR) are more efficient. The BLSR type optical rings are referred to as shared protection rings (SPRINGS). The various OMS SPRINGS are similar to the versions of SONET BLSRs. The SONET four-fiber rings typically have span protection. However, this may not be true with WDM rings.

The OCH SPRINGS do not have a counterpart in SONET rings; there would be too many possible point-to-point paths through bi-directional rings for bidirectional path switching. SONET rings do provide protection selectivity where protection switching in a BLSR can be turned off for specific client signals. Protection selectivity is one motivator to use OCH protection mechanisms in WDM rings. 4F OCH SPRING without span protection is essentially the same as the two-fiber case.

For the objectives of this project, OCH DPRING topology with emulated 1+1 protection scheme is considered for network configuration.

2.4.2 OCH DPRING Function

Figure 2 shows a diagram of an OCH DPRING. In this ring, the dedicated 1+1 protection scheme is used; both working and protect signals are delivered through the ring on different fibers. For example, working traffic from node A to node C travels counterclockwise around the ring; traffic from C to A travels in the same direction on the same fiber. As a result, each optical channel requires a dedicated wavelength throughout the ring.

Each wavelength that is added at an ingress node is optically split and multiplexed for transmission over both fibers. At the egress node, the dropped wavelengths are optically demultiplexed from both fibers. For each wavelength, a comparison switch selects the best incoming optical signal: working or protect. The operation of the OCH DPRING is similar to a SONET UPSR ring. However, the critical add-drop functionality, multiplexing, demultiplexing, and protection switching, is performed in the optical domain, rather than the electrical domain.

A detailed view of the optical add-drop functionality of OCH DPRING is shown in Figure 3. The first requirement of the WADM is providing access to wavelengths that must be added or dropped at a particular node. In this model, an optical demultiplexer, such as a grating-based device, is used to split apart all of the wavelengths on the ring for potential processing at the node. A 2x2 optical switch for each wavelength is used to determine whether incoming signals on that wavelength should be allowed to pass through the node, or whether they should be dropped and replaced by new signals. For example, node C drops the signals arriving from node A, and then inserts its signals destined for node A.

To feed signals to both fibers, an optical splitter is required for each added wavelength. A comparison switch is required for each dropped wavelength.

NOTE: Assuming symmetrical bidirectional connections between nodes, a signal will be added for each dropped signal. The outgoing signals are then multiplexed for transmission to the next node.

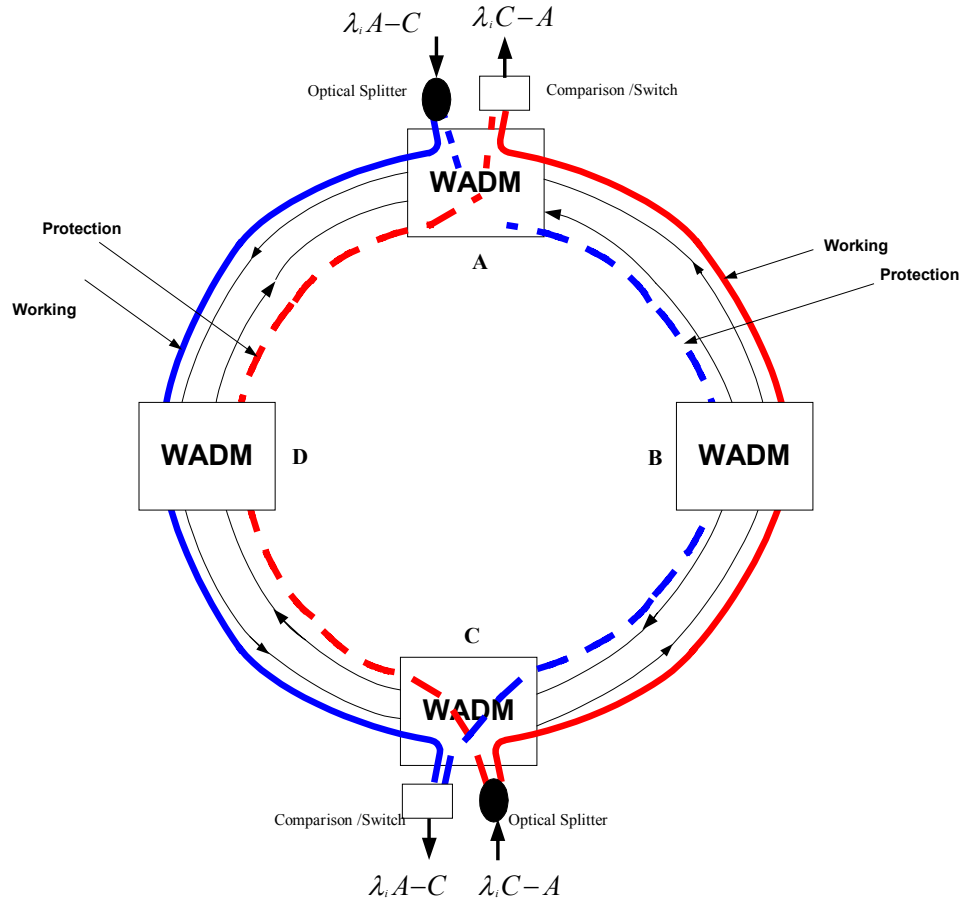


Figure 2 OCH DPRING

For long reach networks, a pair of optical fiber amplifiers (OFAs) may be required at each node to compensate for optical power losses due to signal attenuation. Attenuation occurs within the WADMs and on the fiber links connecting the nodes.

2.4.3 Protection in Multi-ring Optical Networks

For multi-ring optical networks, two types of protection architecture are defined by ITU-T: *trail protection* and *subnetwork connection (SNC) protection* [1]. It is important to consider both individual rings, and interconnections of rings and OCH trails that span multiple rings. OCH ring interconnection would be configured analogous to the SONET/SDH ring interconnection architectures as described in ITU-T G.692 [2].

If the OCH trail protection architecture is used, then the overall end-to-end OCH trail is protected. If the OCH SNC protection architecture is used, then each sub-network independently applies its own protection procedure. For example, in a 3-ring network, with a failure in Ring 2, Ring 2 would exercise its SNC protection, and no actions would be required from Rings 1 and 3, or from the OCH trail termination points.

If OCH SPRINGs are used with OCH trail protection architecture, a very complicated procedure will be required between the OCH trail termination points and the individual SPRINGs. The OCH trail termination points will need to detect the failure and manage the protection switching, but communication with the individual rings will be necessary to identify where the failure has occurred and for configuring shared protection resources.

With the SNC protection architecture, a single ring protection protocol can be extended in a straightforward manner to handle interconnected rings. For this reason, the SNC protection architecture has been recommended for the OCH SPRING in ITU-T [3].

2.5 Grooming Optical Networks

Previously stated in Phase II interim reports, the issue of the traffic grooming problem for WDM/SONET ring network was studied extensively in this project. This section presents a summary of final results. The study of optical network grooming consists of two parts.

First part: Study the single ring case and provide new formal mathematical problem specifications on some variations of the WDM/SONET ring architecture. The problems were found to be integer linear programming (ILP) problems. Due to the nature of these problems, solving the ILPs directly with exhaustive search method may not be practical for current computational capability. Instead, two heuristics are proposed to determine the near-optimal solutions for different network architectures. To the best of our knowledge, one random search heuristic, based on *simulated annealing* algorithm, has reached the best networking savings in its class. The conclusion is that the multi-hop approach usually achieves superior ADM savings when the grooming ratio is large. However, more wavelengths are consumed.

Second part: Preliminary work on traffic grooming in interconnected ring networks. Three strategies are proposed for interconnecting double rings. For each interconnection strategy, the problem is successfully broken down into several independent small problems each on a single ring network. Although the small problems can be solved by the heuristics proposed in the first part of the study as well, the heuristics are usually inefficient when they are applied to some of the rings because these rings inherently have very special traffic patterns. Two new heuristics are proposed and the three interconnection strategies are compared in terms of the network cost. Some preliminary results on traffic grooming on interconnected multi-ring networks are provided.

The problem of saving ADMs in WDM/SONET ring network through using WADM was first addressed by O. Gerstel, etc. [7], [8] from Tellabs in 1998. More work was conducted by other research groups from MIT Lincoln labs [9], AT&T labs [10], Bellcore [11], etc. This research clarified that the general traffic grooming problem is NP-complete and there is no simple strategy for achieving maximal saving. Most of these studies on traffic-grooming problem focused on single ring network with uniform traffic.

The work began with non-uniform traffic. In the first part of the work, the single ring case was considered. We provide a formal mathematical problem specification for the traffic-grooming problem on WDM/SONET ring network. Several variations of ring architectures are included in this work. Also proposed are two heuristics to find the near-optimal solutions for different network architectures. The effect of different network architecture on network cost is also studied.

In the second part of the study, some preliminary work was performed on traffic grooming in interconnected ring networks. Three strategies are proposed for interconnecting double rings. For each interconnection strategy, the problem is broken down into several independent small problems, each on a single ring network. Due to the special traffic in these small rings, two new heuristics are proposed and the three interconnection strategies are compared in terms of the network cost. Some preliminary results on traffic grooming on interconnected multi-ring networks are also covered.

2.5.1 Efficient Grooming in WDM Ring Networks

In a single WDM/SONET ring network, each wavelength running at the line rate of OC-N can carry several low-speed OC-M ($M \leq N$) traffic channels in TDM fashion. Note that for non-uniform traffic, each connection can have a different OC-M rate. The traffic demand, an integer multiple of the timeslot capacity between any two nodes, is established on several TDM virtual connections. A virtual connection needs to be added and dropped at only the two end nodes of the connection. As a result, the electronic add-drop multiplexers (ADMs) at intermediate nodes, if any, will electronically bypass this timeslot. To continue using existing electronic equipment, it is possible to have some nodes on a wavelength in which

no add-drop is necessary in any time slot. In a static, possibly non-uniform traffic pattern, the savings can be maximized by carefully packing the virtual connections into wavelengths.

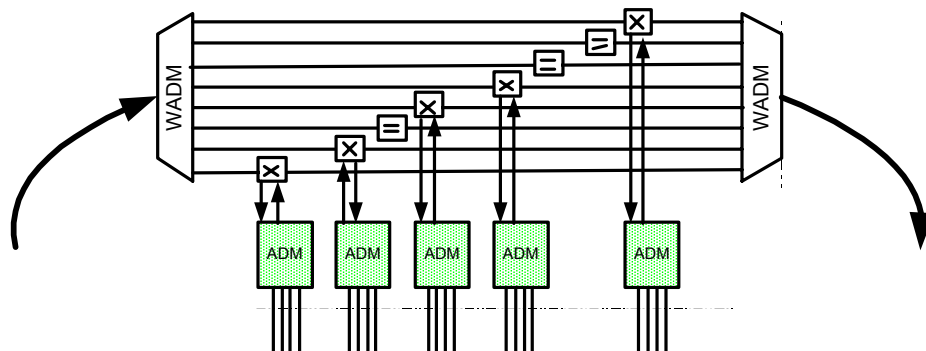


Figure 3 Node Architecture of WDM/SONET Ring Network

Figure 3 illustrates a diagram of node architecture for a general WDM/SONET ring network. Typically, a SONET ring only uses ADMs to finish all the traffic add-drop functionality. This ring is referred to as *single-hop* ring. Simplified node architecture of a single-hop WDM ring is shown in Figure 3; only one fiber is illustrated. In actual situations, there are two fiber rings: one ring for each set of equipment for each fiber.

At each node on each wavelength, a WADM—a 2×2 optical switch, is used to selectively add or drop the wavelength. The wavelength being optically dropped to an ADM, in which some TDM timeslots may be dropped to local stations and some others, may be added back to the wavelength. Figure 3 shows a wavelength that optically bypassed this node because it does not carry any traffic that is destined to or originated from this node. In addition to the single-hop case, the multi-hop ring was considered for an alternative architecture.

In the case of the multi-hop ring, there is a hub node that has as many ADMs as there are wavelengths. A connection can be bridged to different wavelengths and timeslots when passing through the hub node. Any traffic can go through the hub node once. With this hub node, traffic can be groomed at the electronic level; more savings are expected.

2.5.2 Problem Definition

These are the notations for the equations that follow:

- N Number of nodes in the network
- W Number of wavelengths in the network (each wavelength can transmit several timeslots in time-division fashion)
- C Wavelength capacity, which is the number of timeslots a wavelength can carry (also, referred to as the grooming ratio)
- $T(t_{ij})$ Non-uniform traffic matrix, in which t_{ij} represents the traffic from node i to j
- $V_{ij}^{cw}, {}^A V_{ij}^{cw}, {}^B V_{ij}^{cw}$ Virtual connection from node i to node j on timeslot c , wavelength w . V_{ij} is used in a unidirectional ring since there is only one legal direction. ${}^A V_{ij}$ and ${}^B V_{ij}$ are used in a bidirectional ring and they represent the clockwise and counter-clockwise virtual connections, respectively.
- O_i, I_i In the multi-hop case, O_i represents the virtual connection that starts from node i and terminates at the hub node. Similarly, I_i represents the virtual connection that starts from the hub node and terminates at node i .

ADM_i^w	Number of ADMs at node i on wavelength w
e	A link on the physical ring
Given	A set of wavelengths, each with C timeslots, and each timeslot has one unit capacity; a non-uniform traffic matrix T

All traffic demands must be carried by one or more timeslots. The objective is to minimize the total number of ADMs in the network. The traffic-grooming problem for a unidirectional ring can be mathematically specified as shown below.

Objective function: Minimize $\sum_i \sum_w ADM_i^w$

$$\begin{aligned}
\text{Subject to: } \sum_w \sum_c V_{ij}^{cw} &= t_{ij} && \dots \forall i, j && \text{(Traffic load constraint)} \\
\sum_{\substack{w \\ [e \in (i, j)]}} V_{ij}^{cw} &\leq 1 && \dots \forall e, c, w && \text{(Timeslot capacity constraint)} \\
\sum_c \sum_j V_{ij}^{cw} &\leq C \cdot ADM_i^w && \dots \forall i, w && \text{(Transmitter constraint)} \\
\sum_c \sum_i V_{ij}^{cw} &\leq C \cdot ADM_i^w && \dots \forall j, w && \text{(Receiver constraint)}
\end{aligned}$$

Bounds: All V_{ij}^{cw} and ADM_{ij}^{cw} are integers and can be either 0 or 1.

V_{ij}^{cw} The number of virtual connections from node i to node j on timeslot c , wavelength w

ADM_i^w The number of ADMs on wavelength w at node i

Since each timeslot has one unit capacity and there is at most one ADM on each wavelength at each node, V_{ij}^{cw} and ADM_{ij}^{cw} can only be either 0 or 1.

The traffic load constraint states that the summation of all virtual links from node i to node j on all timeslots is equal to the traffic specified in the traffic matrix. The timeslot capacity constraint requires that any timeslot carry only one connection on any given link. The last two constraints specify that the number of virtual connections that start and terminate at any node is bounded by the capacity of the electronic equipment at that node. If there is an ADM, at most C connections can start and terminate there; otherwise, no add drop can occur.

Similar to the single-hop unidirectional ring case, traffic-grooming problem in single-hop bidirectional ring, multi-hop unidirectional ring and multi-hop bidirectional ring are also shown in *Improved approaches for cost-effective traffic grooming in WDM ring networks: non-uniform traffic and bidirectional ring* [12].

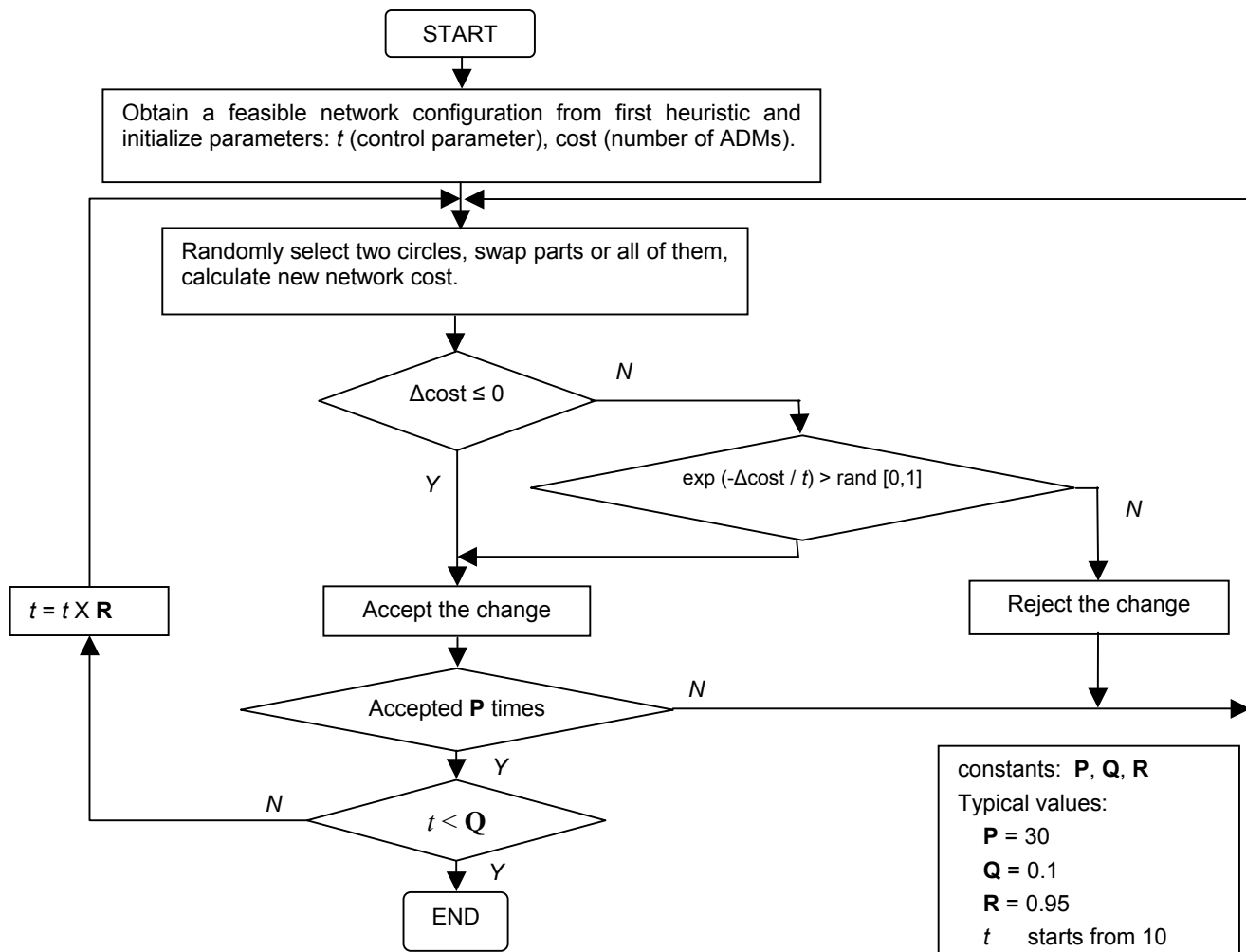
Although proven that the general traffic-grooming problem is NP-complete [9], solving the ILPs directly with an industry strength software package *CPLEX* was attempted. Experiments confirmed the fact that the exhaustive search method will not find an optimal result in reasonable time for even moderate size networks.

2.5.3 Heuristics

Proposed are a simulated-annealing algorithm for single-hop connections and a simple heuristic for multi-hop connections. The heuristic for multi-hop connection is a *Greedy* heuristic. Due to the limitation of the size of this report, only the simulated-annealing algorithm is described in detail.

To control the problem size for heuristic design, the traffic-grooming problem is typically separated into two parts. In the first part, the traffic demands are assigned to minimal number of timeslots. In the second step, the timeslots are regrouped and reformed to construct the wavelength. The first step heuristic was built on the wavelength-assignment algorithm proposed in *An Effective and Comprehensive Solution for Traffic Grooming and Wavelength Assignment in SONET/WDM Rings* [11]. In the second heuristic, a new heuristic is proposed that is based on *simulated annealing algorithm*. This heuristic is to search for possible combinations that achieve maximal savings. The implementation of simulated annealing follows the Monte Carlo method [13], referred to as the Metropolis Algorithm. The algorithm is illustrated in Figure 4.

Figure 4 Simulated Annealing Algorithm



2.5.3.1 Illustrative Numerical Results and Comparisons

This section discusses the heuristics that were tested and developed for single-hop and multi-hop approaches.

Single-Hop Approach

The uniform traffic case has been well studied before in other literature. To evaluate this heuristic, the results obtained by IFOS algorithm were compared with others. In *IEEE/OSA Journal of Lightwave Technology*, [10], the author claimed to have reached the true optimum for uniform traffic on bidirectional rings. Figure 5 shows the results. The results are the same as in that IEEE/OSA article [10] except for one point: N=9 and C=4. IFOS' algorithm saved one additional ADM.

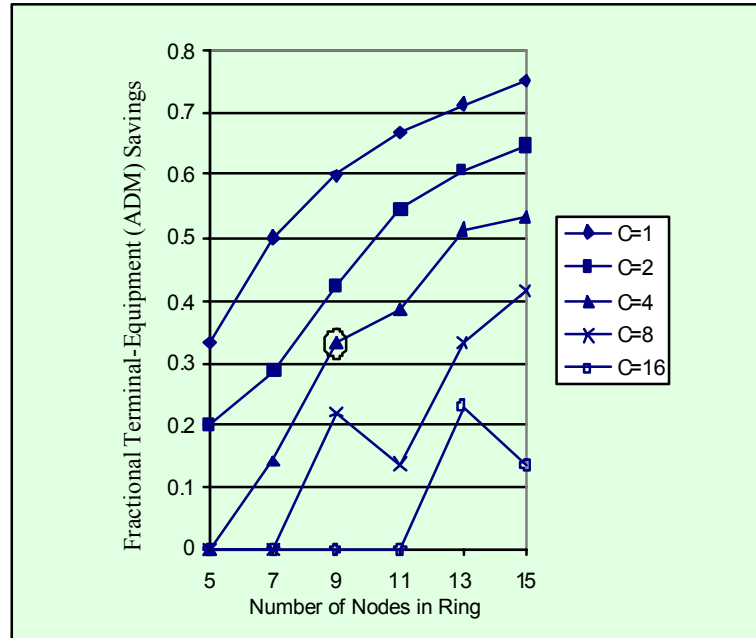


Figure 5 Fractional ADM Savings for a Ring with Uniform Traffic

Figure 6 shows an example that is small enough to be solved by an ILP solver within a reasonable time. A 4-node ring network with a random traffic matrix was selected: $\{\{0, 1, 8, 4\}, \{12, 0, 3, 9\}, \{1, 2, 0, 2\}, \{4, 1, 7, 0\}\}$.

For this network, the grooming ratio (wavelength capacity) was selected as 3. All three heuristic programs were executed: ILP, Simulated Annealing, and Greedy. After six hours, ILP provided its result: 15 wavelengths and 31 ADMs. Simulated Annealing provided the same result in approximately 2 seconds. The Greedy algorithm calculated 33 ADMs in negligible time.

Results from Simulated Annealing are displayed in Figure 6. In this figure, each wavelength is represented by three lines: C=3, each of which represent a timeslot channel; also, G=3. The four nodes on the ring are denoted as nodes 0 through 3. As an example, the 8 units of traffic from node 0 to node 2 are carried by wavelength 4, wavelength 9, and timeslots 2 and 3 of wavelength 7.

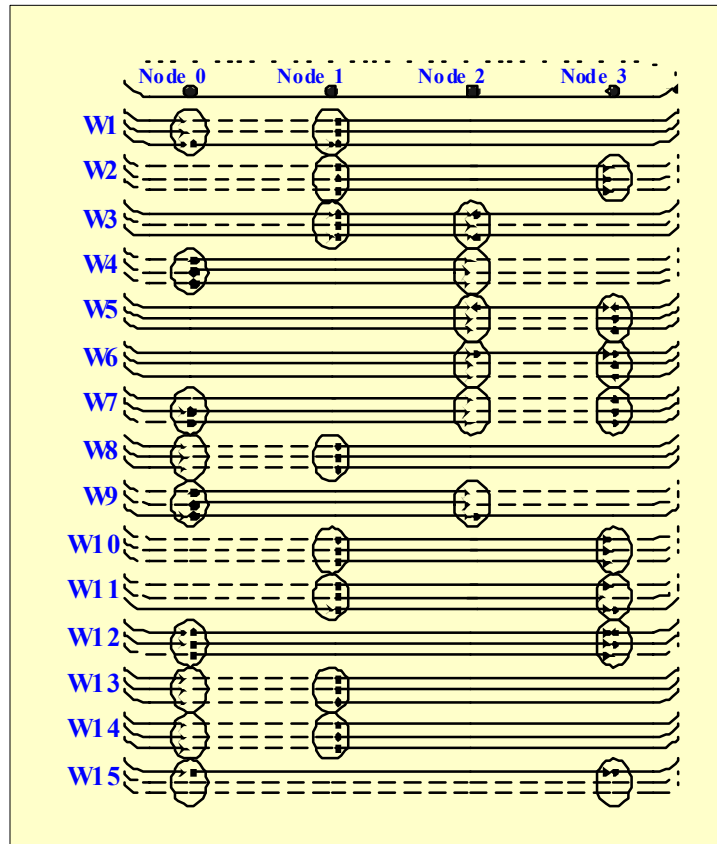


Figure 6 Non-Uniform Traffic Example.

In Figure 6 dots and arrows represent the start and the end of a virtual connection; circles represent ADMs.

Multi-Hop Approach

Figure 7 compares the multi-hop approach with the single-hop approach, under uniform traffic load for unidirectional ring. When the grooming ratio is large ($C > 4$), the multi-hop approach usually requires fewer ADMs; When the grooming ratio is small ($C \leq 4$), the single-hop approach usually requires fewer ADMs.

In general, the multi-hop approach uses more wavelengths than the single-hop approach. For the multi-hop approach, the ADM savings is achieved when the grooming ratio is large. This is due to the savings achieved by its *cross-connection* feature that exceeds the additional cost at the hub node. The large wavelength usage is due to the longer average length of a virtual connection. Similar results also occurred for non-uniform traffic.

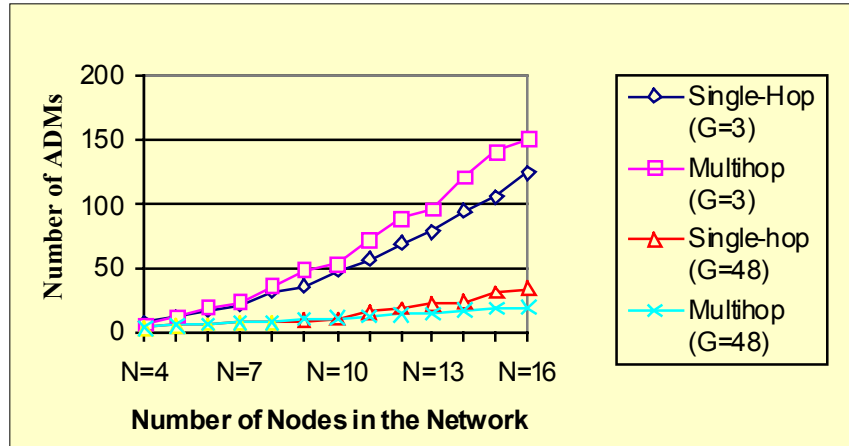


Figure 7 ADM Usage for Single-Hop Connection and Multi-Hop Connection Case

2.5.4 Two Interconnected Rings

For interconnected rings to address fault recovery, at least two physical intersections are desired between two rings. Figure 8 shows a general example of physically interconnecting two rings.

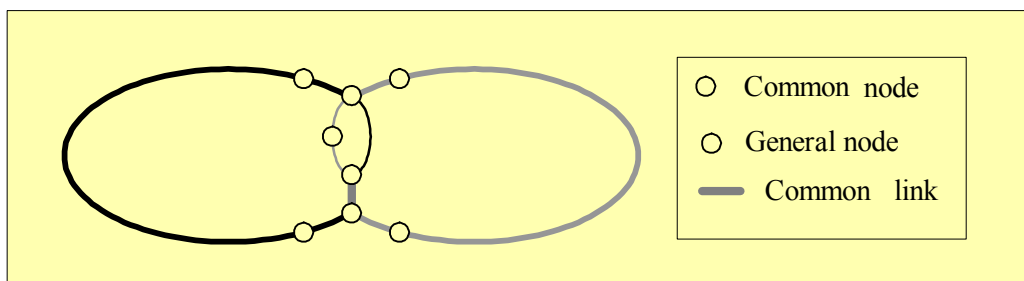


Figure 8 Two Interconnected Rings

Common nodes are the nodes shared by both rings. Traffic that is sourced from or sinked into a common node can be carried through the existing rings, regardless of the location of the other end of the connection.

Traffic between general nodes that are not shared by the two rings can be classified into two categories. If the two ends of the traffic are on the same ring, intra-ring traffic, they can be carried directly on the local ring. If the two ends of the traffic are on different rings, inter-ring traffic, to cover both nodes will require one of the following: a multi-hop approach to bridge the traffic on different rings; a new ring.

Independent of the physical topology, the network can be logically organized differently with cross-connect devices such as digital cross-connect systems (DCS). In this study, if traffic is dropped from one ring to a DCS and is then added to another ring, it is counted as two hops.

2.5.4.1 Strategy 1: DCS at Intersection Nodes (SONET Level Cross-connect)

The first strategy for connecting two rings is connecting them at the SONET level. At each intersection node, a DCS is used to connect the local add-drop ports of some ADMs on the two rings. The function of the proposed DCS is to take lower speed streams (the outputs from some ADMs) as inputs, and then send

them to appropriate input ports on another ring. The DCS is controlled by software and is highly configurable. For simplicity, it is assumed that the DCS has a large number of ports which allows one DCS to be sufficient for an intersection node. Also assumed is that the DCS does not have ADM functionality.

2.5.4.2 Strategy 2: Optical Cross-connect at Intersection Nodes

The second strategy pushes the cross-connect function down to the optical layer. The concept is dedicating some wavelengths to form virtual rings that traverse the boundaries of the physical rings. Virtual rings are used to carry all the inter-ring traffic in the network which requires the capability to optically route some wavelengths across rings at the intersection node. Proposed is using a 3×3 switch on each wavelength at the two intersection nodes that are farthest apart. It is assumed that the major parts of the two rings are disjoint.

Figure 9 (a)—(c) show the details of how this switch can be configured to form virtual rings. Figure 9 (a) shows the configuration in which the light follows the physical ring. Some wavelengths of the WDM network will be configured this way to carry all the intra-ring traffic. In this study, these rings are referred to as *local rings*.

Figure 9 (b) shows the configuration in which two virtual rings carry part of the inter-ring traffic. For a certain class of physical topologies, one of these two rings is sufficient to carry all of the inter-ring traffic. The physical topology of this class of networks has the following feature: every common node of the two rings is also the end of at least one common link — all the common links on the network are contiguous. Essentially, the two rings share one and only one common part where all the nodes are shared, and there are no shared nodes elsewhere. Since all the nodes in the common part are shared by both rings, the traffic between one of them and another node can be carried by one of the local rings. Only one *super-ring* is required to cover all the non-common nodes.

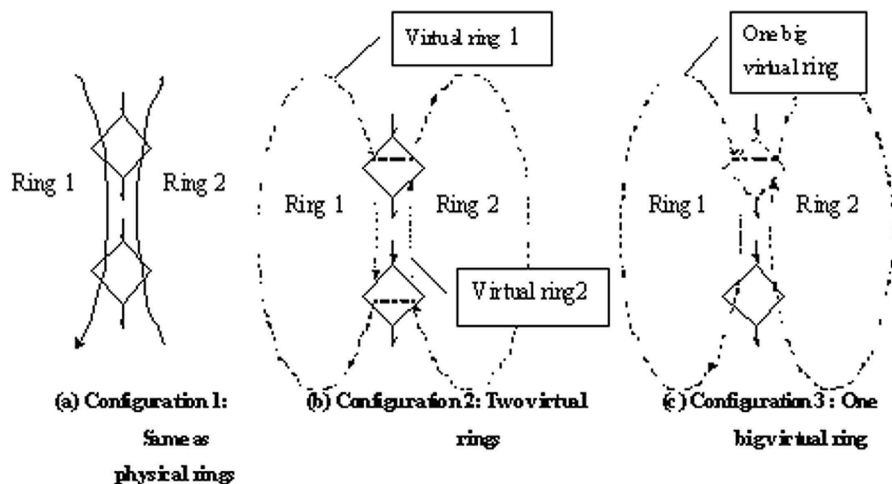


Figure 9 Optical Cross-connect Double Rings

For general interconnected rings, both of the virtual rings in Figure 9(b) will not be able to carry all the inter-ring traffic.

Figure 9(c) shows the configuration that one virtual ring covers all the nodes on both rings. This solves the connectivity problem. However, these two rings have only one common node and if this point fails, the virtual ring will not be recoverable. In addition to the fault recovery problem, this pure optical cross-

connect strategy also suffers from the ring size limitation of BLSR. Because of these problems, this approach is not proposed for general interconnected rings except for the case that the two rings are sharing one common part. Since one *super-ring* can carry all the inter-ring traffic, this case is referred to as the *super-ring* case for all optically-connected double rings. Note that for this interconnection strategy, all of the traffic, intra-ring and inter-ring, will only travel one hop and no OXC is used.

2.5.4.3 Strategy 3: Hierarchical Architecture

This hierarchical architecture, *Mixed SONET and Optical Layer Cross-connect*, is proposed to solve the problems encountered in Strategy 2 and to maintain the advantage of using optical interconnection. In this strategy, dedicated wavelengths are still used to form virtual rings, referred to as *hyper-rings*, which cover some nodes of each ring. At the selected nodes, the local rings are connected to the hyper-ring through DCS. Only the local stations at the logical interconnection nodes can access the hyper-ring directly. Since local stations on other nodes can not access the hyper-ring directly, inter-ring traffic from these nodes must first travel to the logical interconnection nodes through the local ring, and then to the hyper-ring. By doing so, all the intra-ring traffic travels only one hop. Inter-ring traffic may travel between one and three hops.

The one-hop case occurs when the two end nodes are both logical interconnection nodes. The two-hop case occurs when one of the end nodes is a logical interconnection node. The three-hop case occurs when none of the end nodes is a logical interconnection node.

2.5.5 Traffic Grooming in Interconnected Rings

The traffic grooming problem in a single ring is well studied. The basic concept for solving the interconnected ring is breaking the problem into several independent small problems, each on a single ring network. The independent requirement is naturally satisfied as some of the small rings inherently have very special traffic patterns. Heuristics are usually inefficient when applied to some of the rings.

2.5.5.1 Special Traffic Pattern for Different Interconnected Double-Ring Architectures

In the following discussion, an arbitrary, static traffic pattern is assumed. A randomly generated traffic matrix represents the traffic among all the nodes in the network. Each item in the traffic matrix is a uniformly distributed random number between zero and a certain limit.

Optical Cross-connected Rings

The traffic on the three rings, the super-ring and the two local rings, are inherently independent. The traffic pattern on the super-ring is quite different from that of the ordinary rings. The physical intersection nodes are the bottleneck of the super-ring as all the traffic will pass through one of them. Based on the border of the two rings, there is no connection between any node pair within one side of each ring. Therefore, the ordinary traffic-grooming algorithm, most ADMs will only be used for half of their capacity although the other part is still needed for fault-recovery reason. Proposed is a special traffic-grooming algorithm for inter-ring traffic on *super-ring*, discussed in section 2.5.6, Numerical Results and Analysis.

Hierarchical Rings

In this study, only the case in which the hyper-ring has two logical connections with each physical ring is considered. Statistically, the traffic loads among all nodes are evenly distributed. Only the farthest node pairs are considered as the candidates for logical interconnection nodes; they have equal probability of receiving traffic from either side of the ring. This helps avoid wasting wavelengths and ADMs at the interconnection nodes.

Since all the inter-ring traffic goes to the logical connection nodes, and the inter-ring traffic is the dominant component in each ring, there are problems similar as those in the super-ring case. Most of the ADMs are used for only half of their capacity if all the traffic goes to its nearest interconnection node. A new algorithm (heuristic) is proposed to help prevent this problem from happening. This will be discussed

in section 2.5.6.

2.5.5.2 Improved Traffic Grooming Algorithm for Inter-ring Traffic on Optical Cross-Connected Rings

The traffic pattern on super-ring differs from others in the sense that only cross border traffic exists on the ring. An intuitive algorithm for this super-ring traffic is proposed.

2.5.5.3 Improved Traffic-Grooming Algorithm for Hierarchical Architecture

For hierarchically interconnected rings, inter-ring traffic usually is carried to an interconnection node by the local ring. Proposed is an algorithm that tries to evenly distribute the inter-ring traffic along the four possible paths.

2.5.6 Numerical Results and Analysis

Following are discussions of analyses of the Interconnected Double Ring and the Interconnected Multi-Ring.

2.5.6.1 Interconnected Double Ring

To compare the three proposed architectures, two interconnected rings are assumed. See Figure 11. The first ring, *local ring 1*, consists of five nodes. The second ring, *local ring 2*, consists of four nodes. These rings are interconnected at two consecutive nodes. The grooming ratio is assumed to be four. The traffic on the common link is equally assigned to both local rings for all of the architectures. For Strategy 3, the interconnect nodes between the hyper-ring and local rings are fixed; the effects of variations in connection node position are not intended to be studied here. Nevertheless, experiments have shown that the interconnecting position will not statistically affect the result.

Figure 10 shows the average ADM usage for the three proposed architectures, Strategies 1, 2, and 3. This result was obtained from the average of 30 trials. In each trial, a randomly generated traffic matrix was used with each element of traffic ranging from 0 to 16 units. In Figure 11, local ring 3 is the 7-node and local ring 4 is the 8-node ring. The top part for Strategy 2 is the average number of ADMs used by the super-ring. The top part for Strategy 3 shows the average number of ADMs used by the hyper-ring.

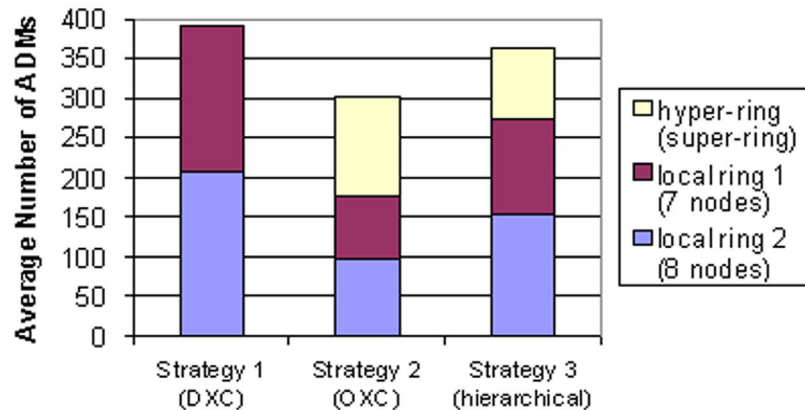


Figure 10 Average Number of ADMs Used for the Three Proposed Interconnecting Strategies

In general, the optically connected architecture (Strategy 2) achieves the best ADM savings. For this architecture, the number of wavelengths used in the super-ring is much more than that in any one of the local rings. The ADMs are also used mainly in the super-ring. IFOS proposed algorithm shows significant

savings. Experiments showed that when using shortest-path routing, the ADM usage on the super-ring will increase about 30% over this result.

The hierarchical architecture (Strategy 3) can not achieve the savings of the optically connected rings. However, significant improvements are seen when compared with the DCS strategy. Considering the ADM usage on the two local rings, the effect of the proposed traffic grooming algorithm is apparent. For these two cases, each local ring must carry all the intra-ring and inter-ring traffic: the traffic load is exactly the same on every local ring for strategies 1 and 3. Note that for Strategy 2, the local ring carries only local traffic. Separating the two interconnection nodes coupled with the proposed traffic-grooming algorithm decreases the ADM usage to a certain level, such that even with the extra cost paid on the hyper-ring, it saves more than the first strategy.

The DCS strategy (Strategy 1) turns out to be the one that saves most on wavelengths. Our calculations also show that the wavelength capacity will not affect the relative ADM usage among the three architectures.

2.5.6.2 Interconnected Multi-Ring

This section discusses the traffic-grooming results for another network topology. The physical topology of the network is shown in Figure 11. Thirty randomly generated traffic matrices are used to evaluate the average ADM usage. Only Strategy 3 uses hierarchical architecture. The hyper-ring, arbitrarily selected for illustration, consists of the following eight nodes: 11, 9, 7, 6, 15, 13, and 1. Note that the nodes 7 and 6 only have connection with ring 2, whereas node 13 is connected to both rings 3 and 4. Figure 10 shows the average number of ADMs that is used in each ring. Unlike previous cases, the number of ADMs on the ring has become the dominant part in the whole network.

The highlights of the results of this section is summarized in Chapter 6.

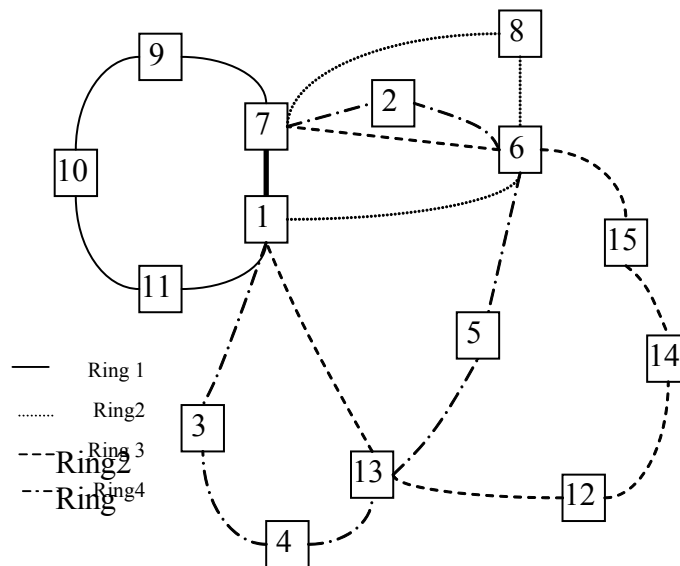


Figure 11 Test Network Topology for Multi-Ring ADM

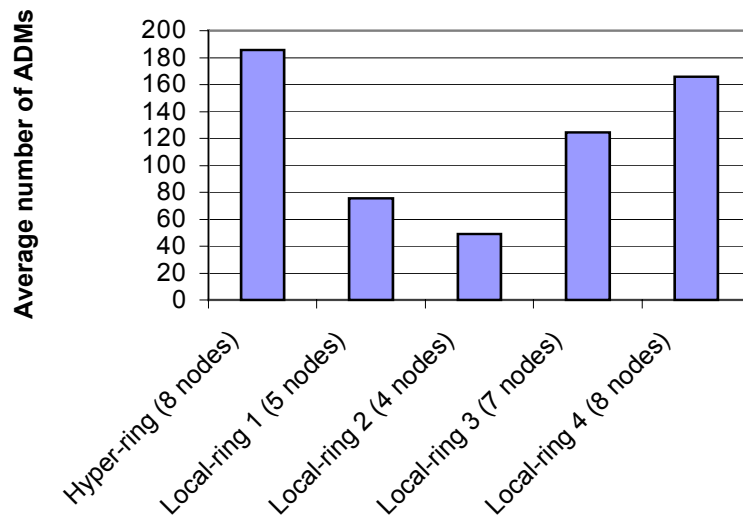


Figure 12 Average ADM usage for a multi-ring network

Chapter 3 WADM Design and Simulation

This chapter discusses the results of the design and simulation of the wavelength add-drop multiplexers (WADMs). After providing a description of the device configuration and the working principle of static and active WADMs, results are presented for a number of studies of the effect of various critical parameters on the performance of the WADM as well as related devices such as: the polished fiber coupler, the attenuator based on a half-coupler with polymer overlay, and the fiber switch based on coupler with polymer interlay. All tree of these devices are precursors and building blocks for the WADM, using most of the elements that go into a full WADM. By studying these devices first, it is possible to gain important insights for design optimization of the WADM. These precursor devices are more easily modeled by today's simulation tools, and they are also more readily produced in the laboratory.

3.1 WADM Overview

WADMs are key devices for WDM or DWDM optical networks. WADMs add-drop a specific wavelength within a group of wavelengths propagating in the network. A specific wavelength is added or dropped by using an optical Fiber Bragg Grating (FBG). These gratings are promising components to be used for these applications; they offer the desired flexible and sharp wavelength filtering characteristics required for these WADM devices.

This discussion is focused on directional coupler based WADMs. The working principle for the device is described, focusing first on the passive device. The dynamic (tunable) WADM is an extension of the passive device, and is discussed in Section 3.1.3.

3.1.1 Working Principle of WADMs

The structure of the directional coupler based WADM is shown in Figure 13. It consists of a pair of matched side-polished fibers with long coupling lengths, L (typically 1-10mm) and two identical Bragg gratings written on both fibers within the interaction length. The identical Bragg gratings have the same values of reflectivity, length, and periodicity. For concentrated reflection, the gratings are placed in the center of the interaction length.

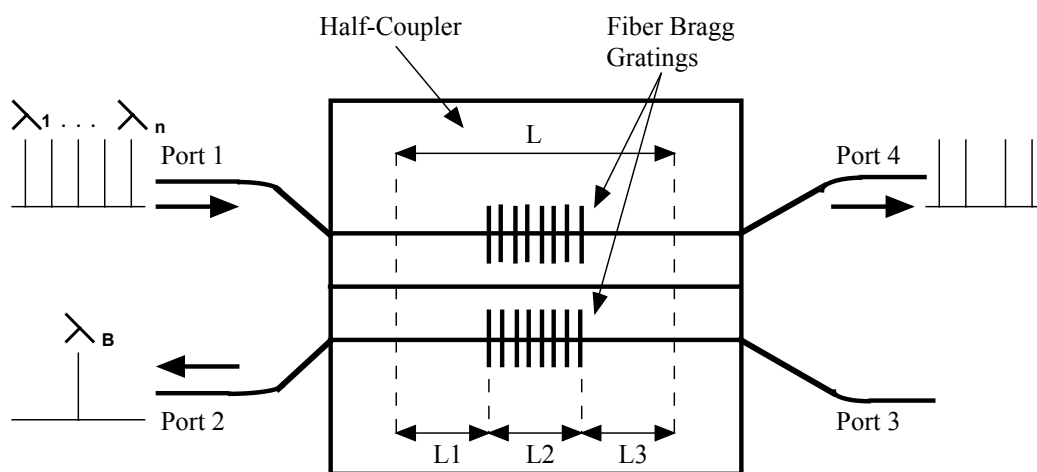


Figure 13 Side Polished Fiber Based WADM

The wavelength multiplexed signal is injected into the port 1 of the WADM. Refer to Figure 13. Within this set of input wavelengths, a specific wavelength (λ_B) that satisfies the Bragg condition is reflected back to port 2. Wavelength λ_B is the dropped wavelength that satisfies the phase matching condition of the following equation:

$$2 K_c L_1 + \delta \varphi = \frac{\pi}{2} \quad \text{equation (1)}$$

Notations:

- L_1 the length of fiber before the grating
- K_c the coupling coefficient of the directional coupler
- $\delta\varphi$ the phase shift induced by the grating

Another wavelength signal that satisfies the Bragg condition of these gratings can be injected into port 3. That wavelength would then be reflected to port 4 as an added signal.

Wavelengths that do not satisfy the Bragg condition are transmitted to port 4 as in a conventional directional coupler (no Bragg gratings), provided the total length of the coupling region ($L = L_1+L_2+L_3$) is equal to twice the coupling length

WADM Modeling Results

The modeling results of normalized power transmission vs. wavelength are shown in Figure 14. It shows the power transmission across the ports 1, 2 and 4 for a WADM of the type illustrated in Figure 13. The output power across port 4 shows that the wavelength λ_B (~ 1535 nm) is dropped. This corresponds to a minimum in the plot of power across port 4 at $\lambda_B = 1535$ nm (see Figure 14). The output power across port 2 shows that λ_B was coupled to this port after being reflected by the grating. It can also be seen in Figure 14 that the sum total of the power in ports 2 and 4 at any wavelength is equal to the power injected into port 1. Figure 14 also shows that the power in port 2 has a sharp and narrow peak.

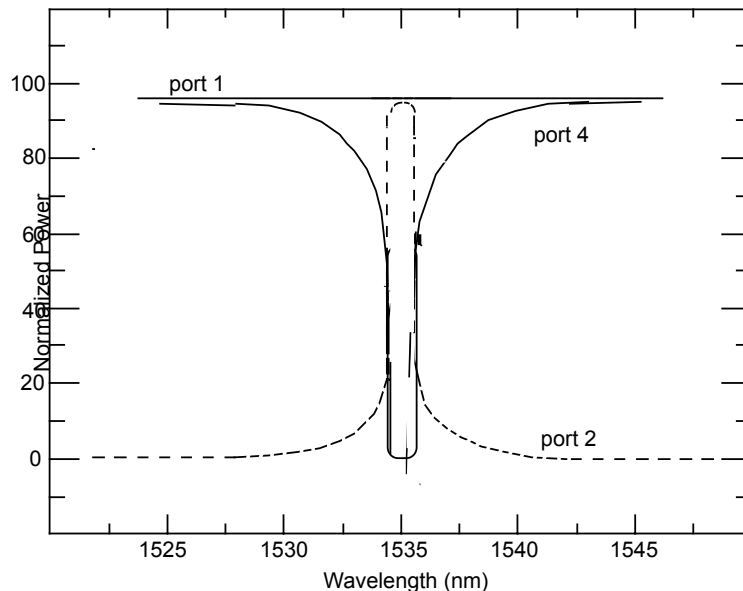


Figure 14 Polished Fiber with Long Interaction Length.

Figure 15 illustrates the comparison of this output with the output power in port 2 from a WADM based on conventional technique: side-polished fiber with a short interaction length. This comparison shows that the conventional technique gives rise to a very broad output, which is not desirable in optical network applications where wavelength channels are very closely spaced. These results indicate the superiority of the long-interaction length IFOS technique.

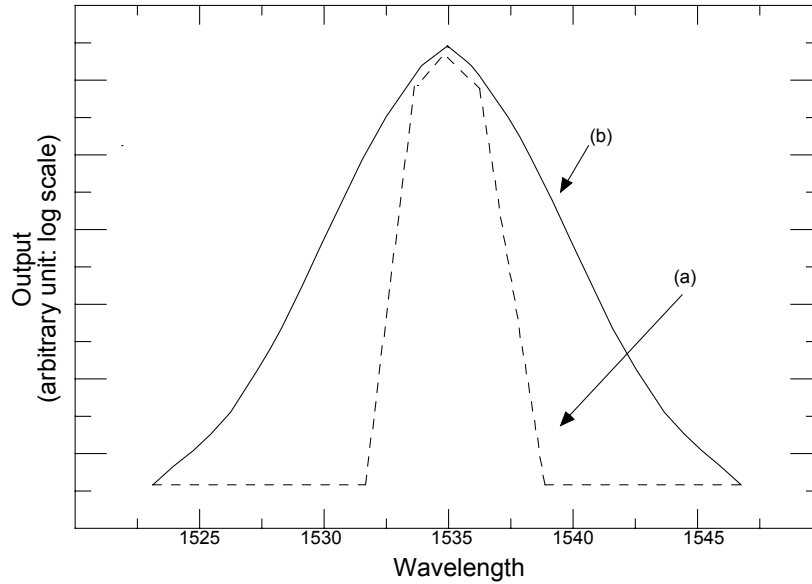


Figure 15 Response in Dropped (Reflected) Port 2

- (a) Side-polished fiber having a long interaction length
- (b) Side-polished fiber having a short interaction length

3.1.2 WADM Advantages: Side Polished Fibers with Long Interaction Length

The technique adopted by IFOS to fabricate directional couplers for WADMs involves side polishing of fibers that have been mounted in Silicon V-grooves. This technique offers a large fabrication tolerance for the device; the tolerance is of the order of the coupling length, L_c (single to few-mm range) for these WADMs. In contrast, the Mach-Zehnder based WADMs only have the fabrication tolerance of the optical wavelength ($\sim 1.5 \mu\text{m}$).

In order to achieve the WADM filtering property described, uniformity is required in the polished region where the two fibers interact. IFOS's polishing uniformity not only enables WADM performance, but also produces devices with negligible insertion losses.

3.1.3 Dynamic WADM

The dynamic WADM accomplishes the same task of adding or dropping signals as the static WADM, but instead of doing so at only one predetermined, fixed wavelength, it can be tuned to drop the desired optical channel. In the language of Section 3.1.1: λ_B , can be adjusted to match the wavelength signal of interest. This is accomplished by adding an optical polymer interlay between the two halves of the WADM directional coupler, as shown in Figure 16. As described in subsequent sections, the operation of the device is governed by the refractive index of this interlay material. The refractive index of the polymer can be tuned using an applied voltage in the case of electro-optic (EO) polymers, and using heat in the case of thermo-optic (TO) polymers. Both types of polymers have been studied in this project.

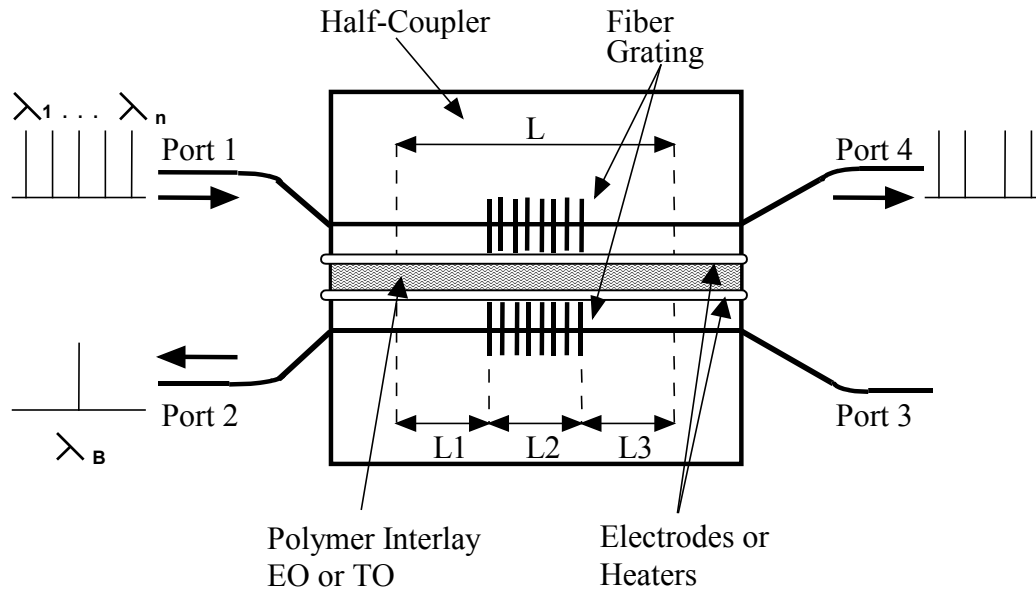


Figure 16 Dynamic WADM Schematic

3.2 Optimized Device Simulation and Design

This section discusses the results and the considerations of device simulation and design.

3.2.1 Device Simulation

This simulation study investigated the sensitivity of power distribution between the SPF and a polymer overlay with respect to several device parameters. The proposed switch design consists of two side-polished fibers (SPFs) with an electro-optic polymer interlay. A correlation function method, based on the Beam Propagation Method (BPM), is used to simulate the wavelength selectivity and the power distribution across the SPF based devices. The device studied is a SPF with polymer overlay.

3.2.1.1 Variation of Remaining Cladding Thickness

The simulation studies on the effect of the variation of remaining cladding thickness on the transmission revealed the following:

- The position of the dip in the transmission curve is independent of the variation in the thickness of the remaining cladding.
- The fraction of power coupled across from the SPF to the polymer overlay is controlled by the thickness of the remaining cladding for a given set of phase matching parameters. When the thickness of the remaining cladding between the SPF and the polymer overlay is smaller, the coupling between the two waveguides is stronger. Result: a larger amount of power is coupled over from the SPF to the overlay and hence the transmission dip broadens.

3.2.1.2 Variation of Polymer Overlay Thickness

The simulation studies on the effect of the variation of the thickness of the polymer overlay on the transmission revealed the following:

- As the thickness of the polymer overlay is increased, the number of guided modes supported by the polymer waveguide increases. This leads to a change in the phase matching condition between the SPF and the polymer overlay. The dip position in the transmission curve shifts to higher wavelengths.

Also, the fraction of power coupled over to the polymer overlay increases. Result: varying the thickness of the polymer overlay changed the shape of the transmission curve and the dip position.

3.2.1.3 Refractive Index of Polymer Overlay

The simulation studies on the effect of the variation of the refractive index of the polymer overlay on the transmission revealed the following:

- As the refractive index of the polymer overlay is increased, the number of guided modes supported by the polymer waveguide increases. This leads to a change in the phase matching condition between the SPF and the polymer overlay. The dip position in the transmission curve shifts to higher wavelengths. The fraction of power coupled over to the polymer overlay increases. Result: varying the refractive index of the polymer overlay changes the shape of the transmission curve and the dip position.

3.2.1.4 Variation of Length

The simulation studies on the effect of the variation of the length of interaction on the transmission revealed the following:

- The radius of curvature of the SPF determines the length of interaction between the SPF and the polymer overlay waveguide. The larger the radius of curvature, the larger the length of interaction. Each device has a coupling length: the portion of the coupling length that is the interaction length dictates the power that is coupled at a specific wavelength.

3.2.2 Design Parameters

This section discusses the studies to obtain optimized design parameters for directional couplers. The areas studied are:

- Coupling ratio vs. s for different interaction lengths
- Polarization dependence in polished couplers

3.2.2.1 Coupling Ratio vs. s for Different Interaction Lengths

Simulations have been performed for directional couplers having interaction lengths of 3, 6, and 10 mm. For a coupler in which the two waveguides (fibers) are parallel and unchanged along the entire length of the device, the coupling coefficient remains fixed; therefore, the optical power just oscillates sinusoidally between the two fibers with a constant period along the length of the coupler. In simulations, one can run the BPM model over just a few mm of the coupler in order to determine the coupling period and extrapolate to determine coupling over any desired interaction length. This method greatly accelerates the study of device performance versus interaction length.

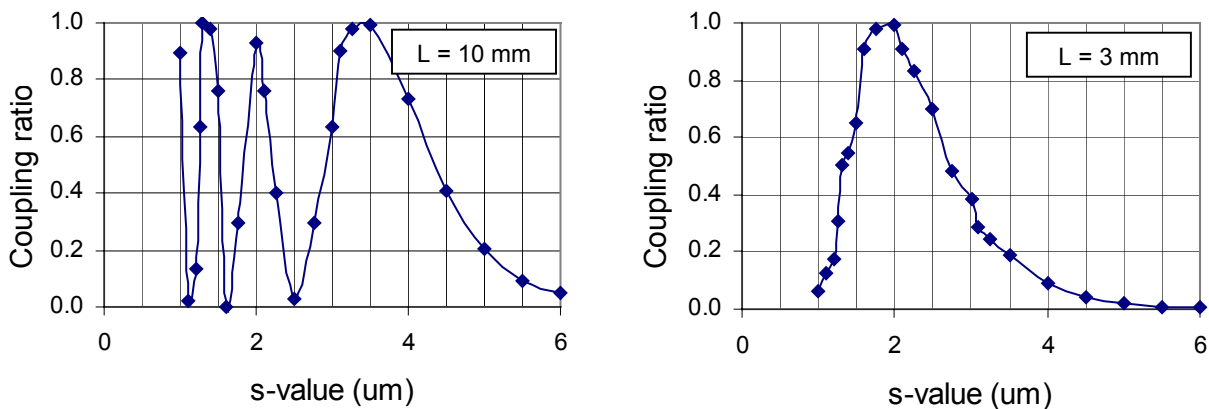


Figure 17 Coupling Ratio vs s for $L = 10\text{mm}$ and $L = 3\text{mm}$

A summary of results for $L = 10\text{mm}$ and $L = 3\text{mm}$ are shown in Figure 17. For $L = 10\text{mm}$, an s value (remaining cladding) of $\sim 4.4\mu\text{m}$ yields 50% coupling, and oscillations occur more quickly as s becomes smaller. Because the fibers are identical, coupling should reach 0% and 100% in each oscillation (they don't in the figures due to the limited number of simulation data points). Examining the results, it is apparent that, as expected, shorter L values require smaller s values to obtain equal coupling.

50% coupling occurs first at $s = 4.4, 3.7,$ and $2.75\mu\text{m}$ for $L = 10, 6,$ and 3mm , respectively. Also, because there is less coupling in shorter devices, fewer oscillations are observed in the plots for shorter L values. Note that the slope of the initial rise from 0 to 100% coupling (moving from larger to smaller s values) is the same for all three L -values. These results indicate that the absolute manufacturing tolerance on s is independent of L . The relative tolerance $\Delta s/s$ is higher for the shorter L values.

3.2.2.2 Polarization Dependence in Polished Couplers

In the simulations thus far, unpolarized input light is assumed. Now, TE (Transverse electric) and TM (transverse magnetic) polarizations are used as inputs for two different parallel-waveguide couplers. Coupler s -values of 4.5 and $2.75\mu\text{m}$ were selected in order to produce around 50% coupling for Interaction Length, $L,$ = 10 and 3mm , respectively.

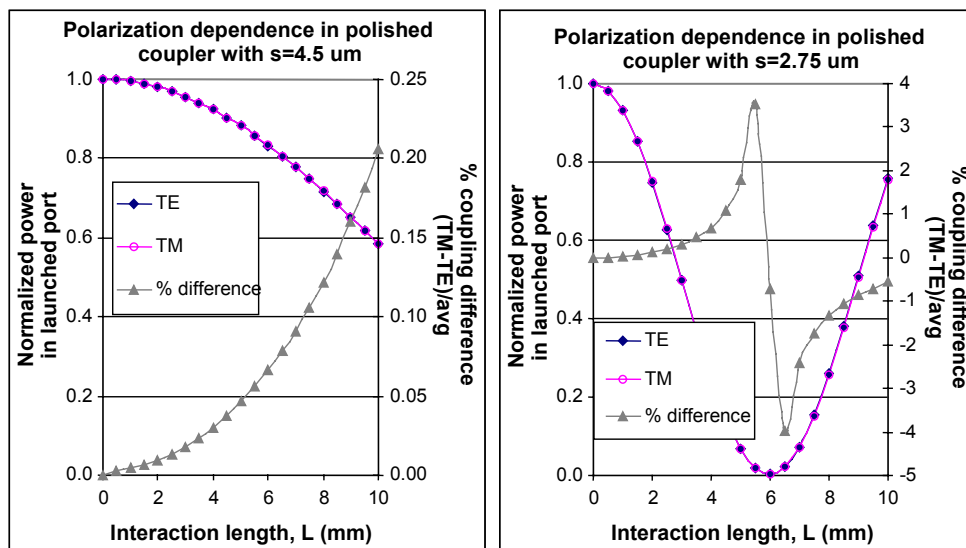


Figure 18 Polarization Dependence of Coupling Ratio for $s = 4.5$ and $2.75\mu\text{m}$

As indicated by the right-side axes in Figure 18, the polarization dependence on the coupling ratio is small. Near the 50% coupling point ($L = 10\text{mm}$ in the $s = 4.5\mu\text{m}$ figure and $L = 3\text{mm}$ in the $s = 2.75\mu\text{m}$ figure), there is $< 0.3\%$ coupling difference between the two polarizations (TM-TE / average) in both cases. The TM polarization couples slightly more strongly, and the difference in coupling (polarization dependence) grows moving down the length of the coupler. For the case $s = 2.75\mu\text{m}$, the coupling difference between TM and TE polarization grows for longer interaction lengths and then changes sign near the point at which coupling reaches 100% ($L = 6\text{mm}$). This is due to the difference in the period of the sinusoidal movement of power between the two fibers. The difference in coupling coefficients between TM and TE causes one polarization to reach full coupling at a different L value than the other polarization. Although interesting from an academic standpoint, this is not important in practice, as a coupler with $s = 2.75\mu\text{m}$ would only need $L = 3\text{mm}$ to reach the desired 50% coupling point.

3.2.3 Optimized Device Design

This section discusses the development of practical application requirements for IFOS WADM by obtaining optimized design rules and parameters. In this section, after a brief introduction on SRF (side

removed fiber), basic design rules for SRF/ICFG (Intra-Core Fiber Grating) with AOP (active optical polymer) are introduced.

3.2.3.1 SRF/ICFG Model

Gratings are key components of the IFOS WADMs. They operate by substantially coupling two modes (equations 2 and 3) when the following phase-matching condition is satisfied:

$$\beta_1 - \beta_2 - \frac{2\pi}{\Lambda} = 0, \quad \text{equation (2)}$$

Where $\beta_1 = kn_{\text{eff1}}$ and $\beta_2 = kn_{\text{eff2}}$ are the propagation constants of the two modes, Λ is the spatial period of the grating, henceforth referred to as the “grating period” with $n_{\text{eff1}} = \beta_1/k$ and $n_{\text{eff2}} = \beta_2/k$ being the effective refractive indices of the two modes, λ the wavelength, and $k = 2\pi/\lambda$ the free-space wavenumber. The wavelength that satisfies the phase-matching condition (at which coupling is maximized) is known as the Bragg resonance wavelength:

$$\lambda_B = (n_{\text{eff1}} - n_{\text{eff2}}) \Lambda \quad \text{equation (3)}$$

In the case of modal reflection, $n_{\text{eff1}} = -n_{\text{eff2}} = n_{\text{eff}}$ and thus the Bragg wavelength, which corresponds to a notch in the transmission spectrum of the grating, is given by $\lambda_B = 2n_{\text{eff}} \Lambda \approx 2.9\mu\text{m}$ for a silica fiber in the 1550 nm wavelength band. The period Λ of a grating written into a fiber and hence the Bragg wavelength, i.e., *notch*, can be changed by stretching/compressing or heating/cooling. Alternatively, λ_B can be altered by changing the effective index seen by the mode.

$$\delta \lambda_B / \lambda_B = \delta n_{\text{eff}} / n_{\text{eff}} \quad \text{equation (4)}$$

This can be achieved by side-polishing the fiber as discussed below. In a first approach to the analysis of SRF/ICFGs, one determines the parametric dependence of modal effective indices of SRFs. Then SRF/ICFGs can be analyzed within a perturbation framework using the proportionality of the Bragg wavelength shift to effective index shift of equation (2). For example, Figure 19 shows the results of numerical finite-difference method solution for the fundamental mode effective index as a function of the minimum spacing between the planar dielectric surface and the center of the fiber core r_{polish} . These results can be used to determine the Bragg wavelength shift

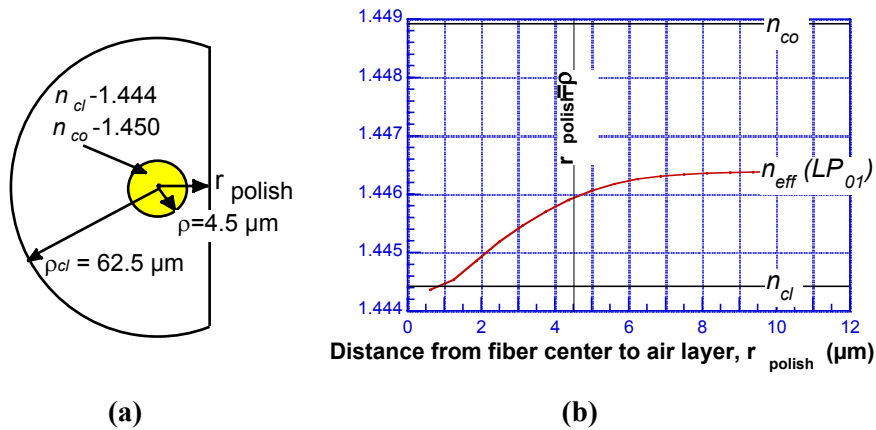


Figure 19 Fiber Parameters

- (a) Side-removed fiber cross-section with parameters for modeling.
- (b) Effective-index change versus distance of polishing from fiber center r_{polish} . Parameters used in the model: wavelength $\lambda = 1.55 \mu\text{m}$; fiber core radius $\rho = 4.5 \mu\text{m}$; fiber cladding radius $\rho_{cl} = 62.5 \mu\text{m}$; core-cladding index difference = 0.0045

3.2.3.2 SRF/AOP Models and Design Rules

This study comprised an AOP planar multimode waveguide overlay which is evanescently coupled to a SRF. The SRF has an electroded AOP overlay waveguide. Refer to Figure 20 which also illustrates the spectra.

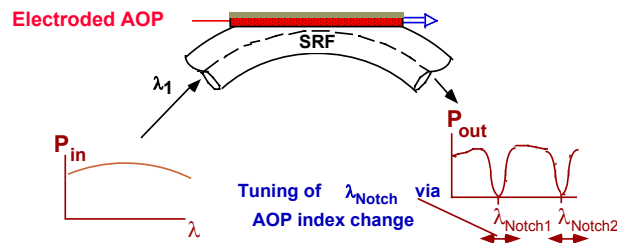


Figure 20 SRF

Figure 21 shows the major features of spectral transmission properties. Notches in the wavelength spectra occur. The most crucial parameters determining number, width and depth of these notches depend on the following:

- AOP overlay thickness
- Distance of overlay waveguide from fiber core as a function of distance along the waveguide
- Core, cladding and polymer indices

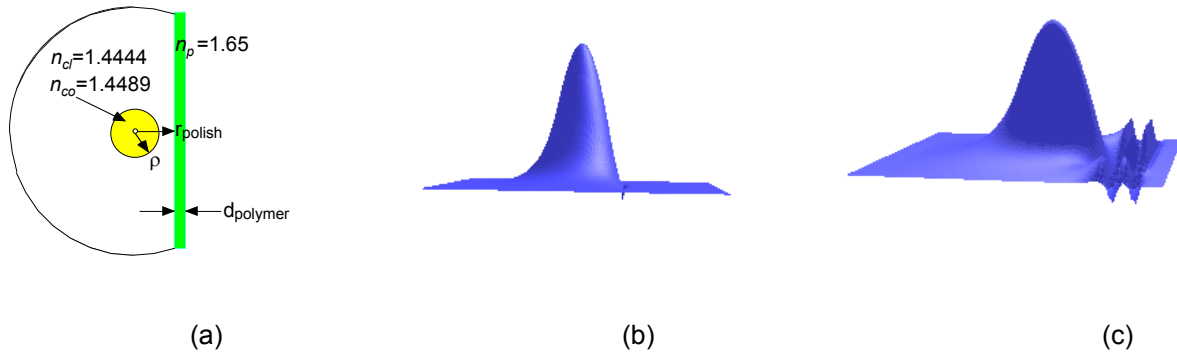


Figure 21 Spectral Transmission Properties

(a) Modeled SRF, and example modal fields (b) away from phase-matching wavelength, and (c) close to a phase-matching wavelength

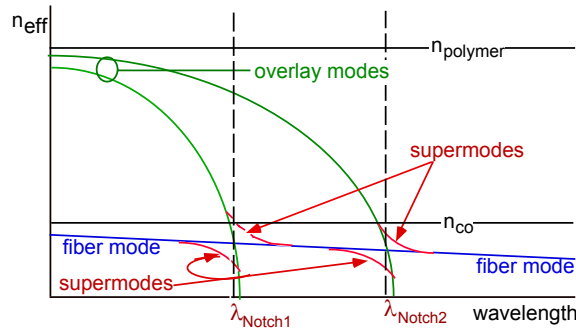


Figure 22 Fiber and Overlay Substructures

Figure 22 illustrates the effective modal indices (n_{eff}) for the modes of the fiber and overlay substructures with the supermodes of the SRF/AOP overlay superstructure shown in Figure 21.

3.3 Device Design

Figure 23 shows the cross-sectional view of a switch. The switch consisting of two side-polished fibers with a polymer interlay. The proximity is a few microns, between the cores of the two SPFs. The refractive index of the polymer is assumed $n = 1.4$. The length of propagation is assumed $L = 5$ mm

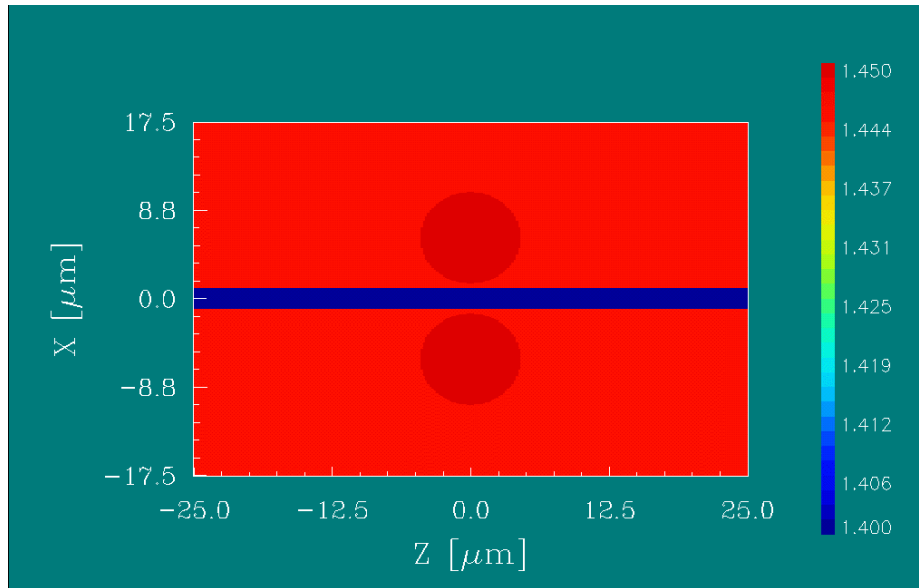


Figure 23 Cross section of a switch. The switch consists of two side-polished fibers and polymer interlay

The electric field amplitude distribution across the switch cross-section is shown in Figure 24. This figure shows that the majority of light is in the upper SPF. The switch has been designed so that this light is coupled to the lower SPF. Coupling light from one fiber to another fiber depends on the coupling length of the switch.

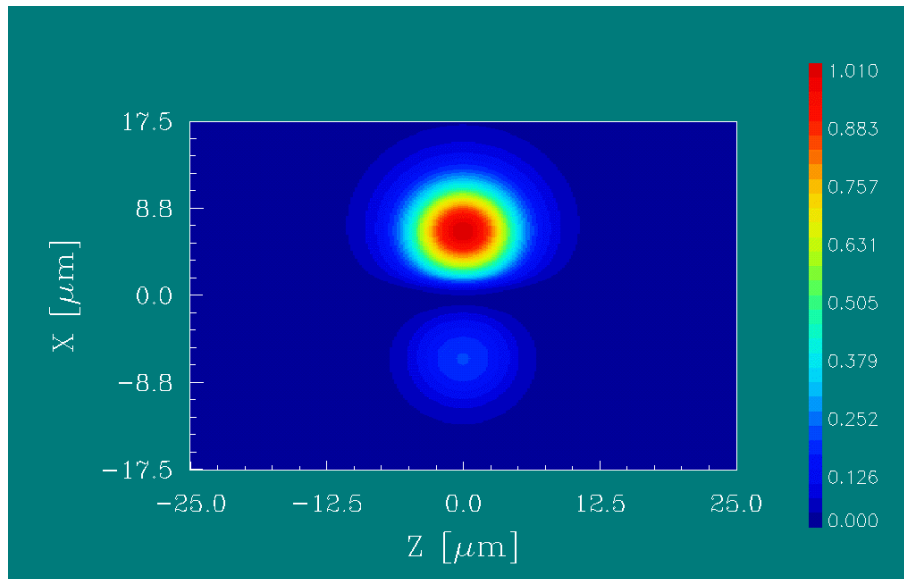


Figure 24 Electric field amplitude distribution in the switch after propagating 5mm.

The direction of propagation of light in the switch is assumed to be Y-direction. Corresponding to the conditions in Figure 24, at $Z = 0 \mu\text{m}$, Figure 25 illustrates the electric field distribution along the Y-

direction. This shows that the light coupled to the lower SPF in the 5mm switch length is very low for the selected set of parameters.

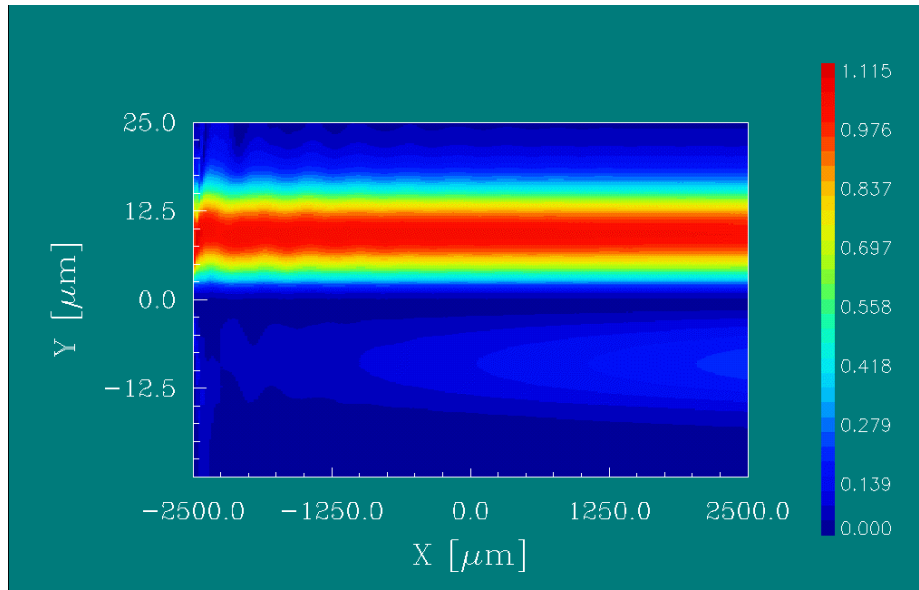


Figure 25 Electric Field Amplitude in the switch in the direction of propagation

3.4 Selecting the Refractive Index of the Polymer

It is very critical to select the value of the refractive index of the polymer for the final device. To start with some numbers, we chose the following parameters for the SPFs within polymer interlay:

- Thickness of overlay, $d = 2 \mu\text{m}$,
- Remaining cladding thickness, $s = 2 \mu\text{m}$,
- Length of propagation = 10 mm

Coupling length is defined as the length of interacting region of coupled guides in which the light is completely coupled from one fiber to the other, then back to the first fiber. This action corresponds to a phase shift of 2π .

This section discusses the variation of coupling length as a function of the variation in the polymer index. As n is increased from 1.43 to 1.45 for $d = 2 \mu\text{m}$ and $s = 2 \mu\text{m}$, the coupling length decreases from 20 mm to 2.35 mm. The field distribution for various refractive indexes of the polymer overlay is shown in Figure 26. The changing coupling periodicity is clearly observed.

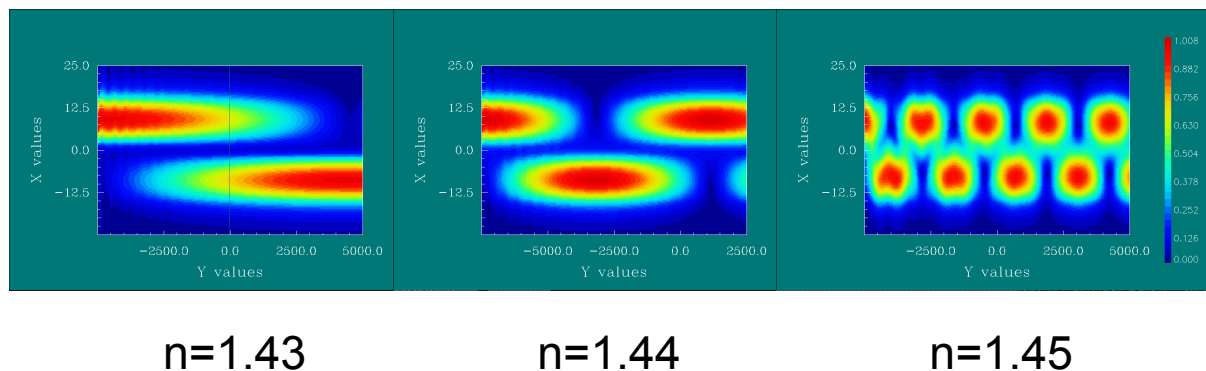


Figure 26 Electric field

Figure 27 shows a plot of the coupling length as a function of the refractive index of the polymer interlay for two thicknesses of the polymer interlay.

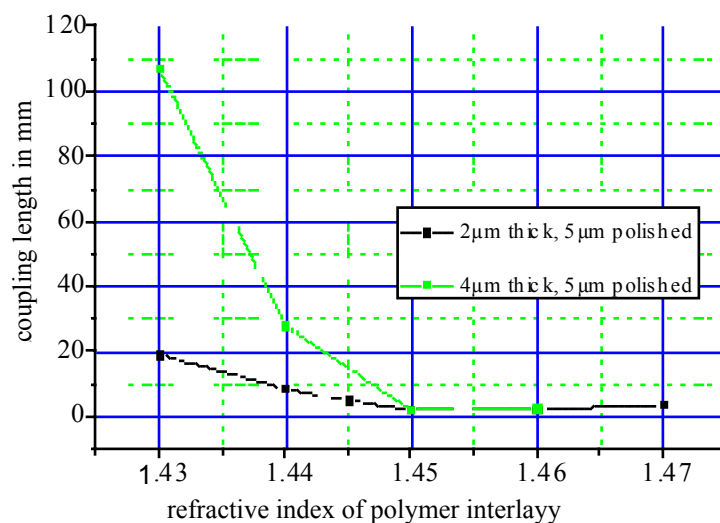


Figure 27 Coupling length as a function of refractive index of polymer interlay.

In the plot shown in Figure 28, the length of interaction = 10 mm is fixed. The variation of phase shift, in multiples of π , is plotted as a function of the refractive index of the polymer. The plot for $d = 4 \mu\text{m}$ shows that if the refractive index of the polymer is varied around 1.445 by 0.001, a phase shift of π occurs: a change in the refractive index of polymer by 0.001 can switch the power from one fiber to the other. The conclusion is that the index of the polymer can be varied either thermo-optically or electro-optically to produce the desired switching.

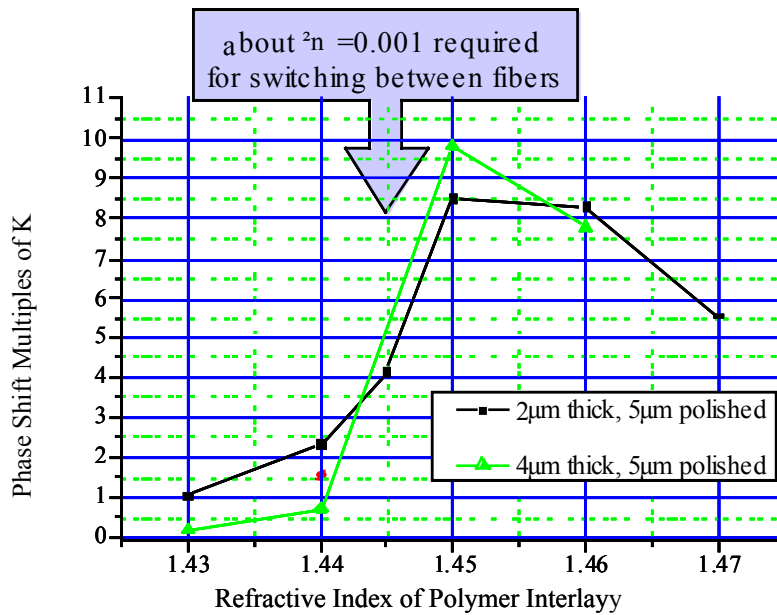


Figure 28 Phase shift in multiples of π vs. refractive index of polymer.

If the refractive index of the polymer interlay is too low (1.4) the interaction length needed to couple light across becomes very large (~ 20 mm). However, if the refractive index of the interlay is higher than 1.45, the waveguide modes of the polymer film are excited. Depending on the thickness of the polymer, strong coupling between the modes will result. This results in substantial energy being present in the polymer film and hinders the desirable coupling of power between the SPFs.

The best choice is a refractive index around that of silica for low switching-voltage applications.

3.5 SPF with Polymer Overlay Power Distribution

The structure of study is based around a side-polished fiber with a small remaining cladding thickness (1-2 μm) and a polymer overlay. It consists of two major components: *Nonlinear Optical Polymer* and *Side Polished Fiber*.

Nonlinear Optical Polymer

The polymer used is P (DR1-MMA) which functions as an overlay. The refractive index is $n = 1.537$ at 1.55 μm , and the thickness is $d = 5$ μm . The switch is tuned by varying the refractive index of the polymer thermo-optically.

Side Polished Fiber

The fiber used is the standard 1.5 μm Single-Mode Fiber (SMF) with refractive index of the core = 1.4499 and the refractive index of the cladding = 1.4444. The core diameter = 8.3 μm . After polishing the fiber, the remaining cladding thickness is $s = 1.1$ μm . Figure 29 shows the refractive index profile of a SPF with polymer overlay, using the parameters previously stated.

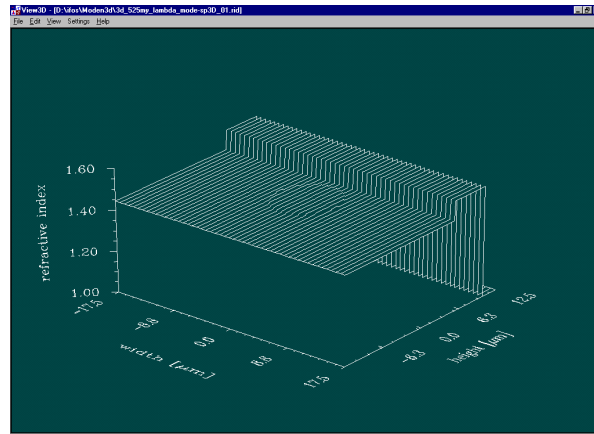


Figure 29 Refractive index profile of an SPF with a polymer overlay.

The light launched in the SPF propagates along the fiber and excites the modes of the fiber-slab device in the side-polished region. In turn, these modes interact with the fiber mode at the end of the polished region. This sets the transmitted power across the SPF for the chosen set of parameters. It is apparent that the transmitted power can be directly tuned by the refractive index of the polymer. In the following sections we report some of these studies.

For the selected parameters, at $\lambda = 1.49 \mu\text{m}$ the fiber mode, effective index = 1.44704, excites two orthogonal modes in the device. The effective indices of the modes of the device are 1.44807 and 1.44623 respectively. The field distributions of these modes are shown in Figure 30 and Figure 31, respectively. These are the two modes that interact significantly with the fiber mode.

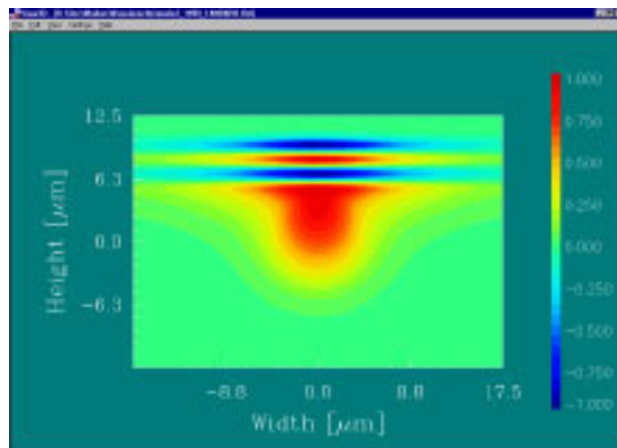


Figure 30 Field Distribution of mode with effective index 1.44807.

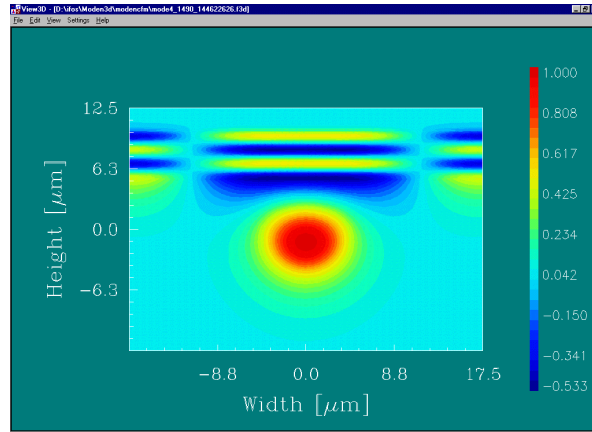


Figure 31 Field distribution of mode with effective index 1.44623.

If both the modes were perfectly bound and no radiation losses occurred then the light could completely couple back and forth between the modes with a coupling length L as shown below:

$$L = \frac{\lambda}{\Delta n}$$

As known from the coupled mode theory, the intensity that is carried by these modes is governed by the overlap integral between the input field, i.e., the fiber mode, and the field distributions of the modes as illustrated in Figure 30 and Figure 31. The input field has to be written as a superposition of the new modes with appropriate complex amplitudes. Because the effective index of each mode is different, the field distribution changes along the propagation direction. The situation with only two waveguide modes can be easily analyzed. If the polymer were structured to form a ridge waveguide, the coupling process could indeed be completely described by these two modes only. For the slab waveguide geometry, however, the situation is more complicated.

The complication is that the polymer modes are not confined to the fiber core; however, there is a continuum of modes in the polymer. During propagation, power is also transferred into these modes. As a consequence, coupling to these higher order modes leads to a loss of power. Hence, the coupling process will not result in a complete energy transfer from the fiber to the polymer as would be the case if only two modes were present.

For the same Power Overlap Integral (POI) curve for the resonant wavelength $\lambda = 1.49\mu\text{m}$, the power in the fiber drops practically to zero after one half coupling length, as expected. Refer to Figure 32 (note the logarithmic y-scale). Also recognized is that the total power in the fiber does not drop completely to zero.

After 1 cm of propagation, 14% of the original power remains in the fiber. This occurs because the first mode (see Figure 30) is still bound to the fiber core and has very little attenuation. In contrast, the second mode (see Figure 31) has a high attenuation because the electric field extends into the whole polymer slab waveguide. The amplitude of this mode decreases with propagation and only the first mode of the compound structure remains.

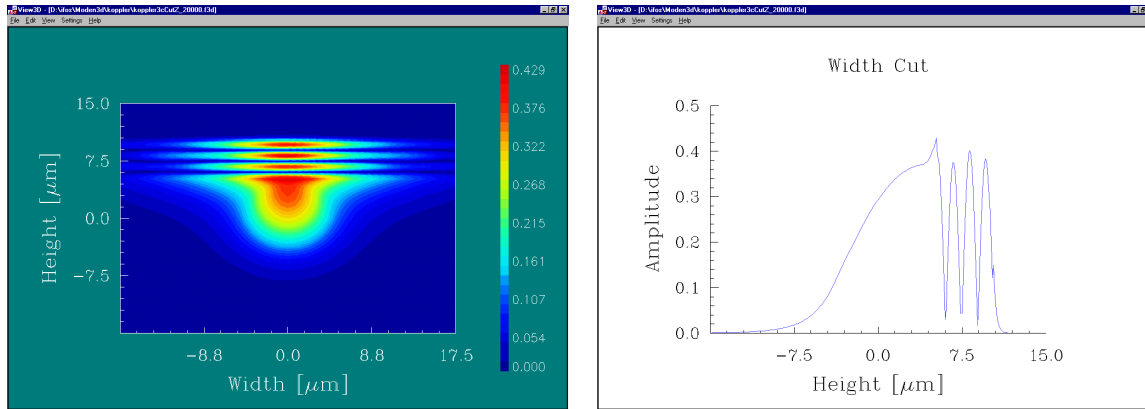
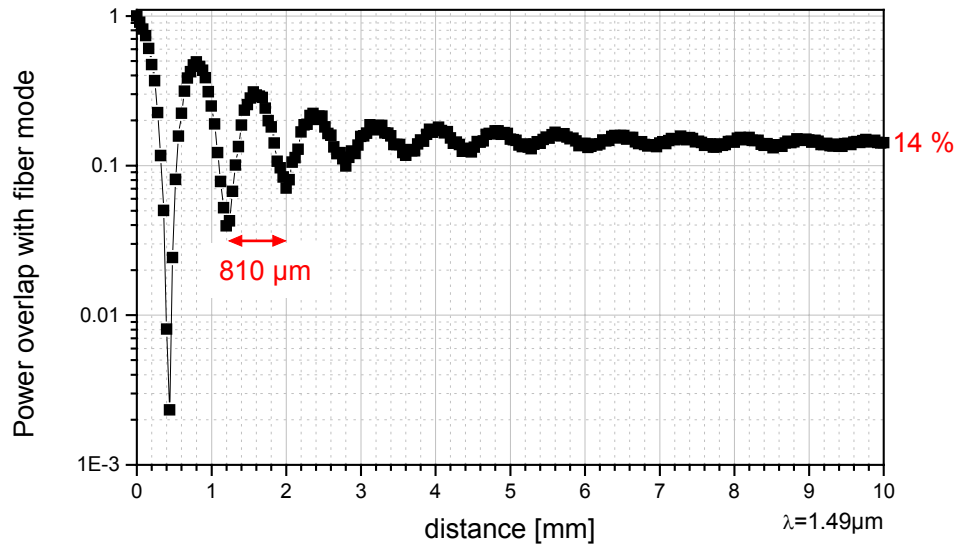


Figure 32 Power Overlap Integral: $\lambda= 1.49$

Figure 32 displays the following:

- Power overlap integral for the resonant wavelength $\lambda= 1.49\mu\text{m}$ vs. propagation distance (top).
- The final electric field distribution is shown on the bottom.
- The confinement inside the polymer is 42%. This mode has very little loss as it is bound to the fiber core.

The confinement factor inside the polymer is relatively high; 42% of the optical power is inside the polymer. This condition is favorable for TO or EO tuning. However, the insertion losses are relatively high: 14% remain in the fiber, which corresponds to 8.5-dB loss. This design needs improvement: the fiber curvature must be taken into account and the entire device must be modeled for precise estimates of confinement and losses. From these results, it is clear that a *low-loss* device cannot be realized with high-index polymers and a simple slab waveguide geometry.

The losses can be accounted for by an additional exponential factor; however, a precise description can only be done numerically.

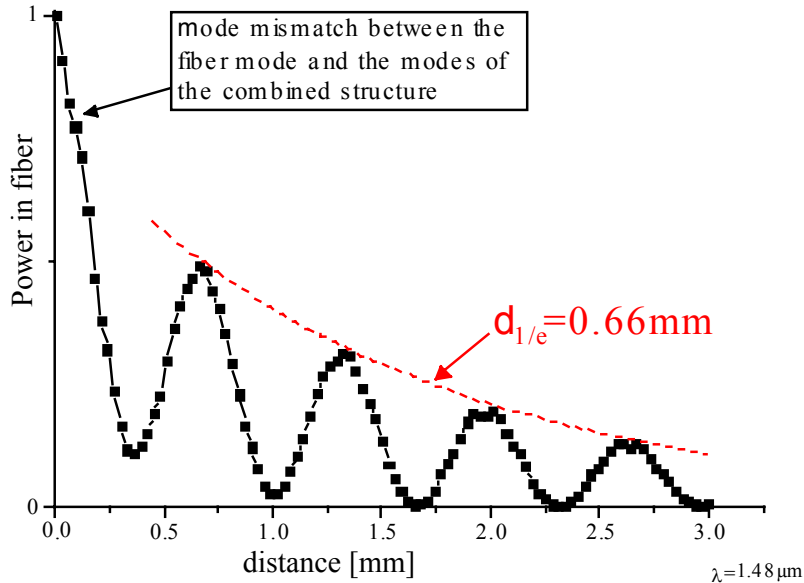


Figure 33 Power Overlap Integral: $\lambda = 1.48$

Figure 33 illustrates the following:

- Power overlap integral between propagating field and fiber mode (excitation field)
- Light couples between the fiber and the polymer with an exponential overall decay due to losses in the slab

In Figure 33, the power overlap integral (POI) between the fiber mode and the propagating field is shown for a distance of 3 mm. The wavelength was slightly detuned from the resonant wavelength ($1.48\mu\text{m}$ instead of $1.49\mu\text{m}$). The reduced coupling efficiency can be recognized (incomplete power transfer: first minimum around 10%) and the changed coupling length ($660\mu\text{m}$ instead of $810\mu\text{m}$). These results show that the device characteristics change strongly close to a resonant wavelength.

This situation cannot be explained with simple coupled wave equations using the modes of the individual waveguides: slab and fiber. Calculating the modes of the *compound structure* is necessary to understand this behavior. However, for little polishing (large remaining cladding thickness s) these modes are very similar to those of the individual waveguides. In this case, an overall exponential decay will be observed. Therefore, small s is needed in order to obtain a situation as described above.

In the plot of power transmission across the fiber as a function of wavelength for a device based on an SPF with polymer overlay we observe the following:

The position of the dip:

- Independent of the remaining cladding thickness, s
- Extremely sensitive to the thickness of the polymer overlay and its refractive index

The polarization dependence of the device arises from the polarization dependence of the polymer waveguide modes:

- The polarization sensitivity decreases by making the device symmetric, e.g., by having another SPF on top of it
- The polarization sensitivity increases by making the device asymmetric e.g., by having air layer above the polymer

3.6 Sensitivity of Power Distribution to the Device Parameters

In Figure 34, the power inside the fiber core has been calculated for a propagation distance of 1 mm for a straight geometry: $R = \text{infinity}$. Each dip in the curve 1 corresponds to the coupling of fiber mode with a new mode in the polymer waveguide, curve 2. Curve 3 shows the sum of both curves. It decreases with wavelength because the fiber mode has less confinement to the core for higher wavelengths. In addition, part of the power is irreversibly lost when coupling to the polymer slab occurs, as indicated by the dips in the curve 3.

To compare the losses for various wavelengths, the power will no longer be taken from inside the waveguide boundaries; instead, the power overlap integral between the propagating field and the fiber mode will be examined. This curve will always be normalized to 1 and not show a decrease with wavelength.

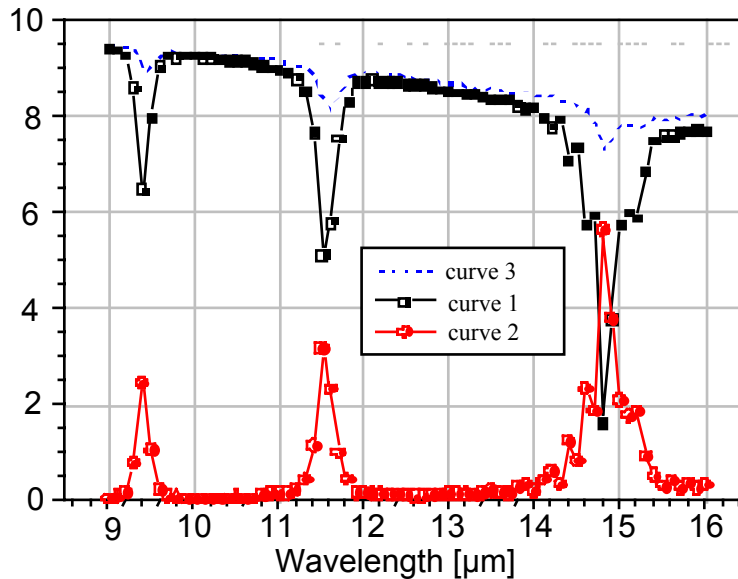


Figure 34 Power Distribution

Figure 34 illustrates relative power in fiber core (curve 1) and polymer (curve 2) versus wavelength for a remaining cladding thickness of $s = 1.1 \mu\text{m}$ and a propagation length of 1 mm. Curve 3 shows the sum of both curves. The variable s , which is the remaining cladding thickness, is the distance between the top of the core and the surface of the uncoated coupler: i.e., the bottom edge of the polymer layer.

The above example was calculated for a straight-fiber geometry, which is convenient to obtain a first impression of the device characteristics. Next: simulate the behavior of a real SPF, with a radius of curvature of $R = 12$ meters. For this case, the total propagation length must be 2cm in order to completely describe the coupling process. The focus will be on the dip near $\lambda = 1.5 \mu\text{m}$.

3.6.1 Effect of Remaining Cladding Thickness Variation

Figure 35 shows the calculation of the transmission characteristics as a function of wavelength for various values of remaining cladding thickness. Looking at curve 1 first, notice that the longer wavelength side shows a steep drop from a transmission of 1 at $1.52 \mu\text{m}$ to 10^{-5} at $1.505 \mu\text{m}$. It is clear that the overall losses are much higher for these long propagation lengths than for the example in Figure 34. The short wavelength side does not have such a steep dependence but is instead broadened. Both curves reach 100% transmission 1 is reached near $\lambda = 1.4 \mu\text{m}$.

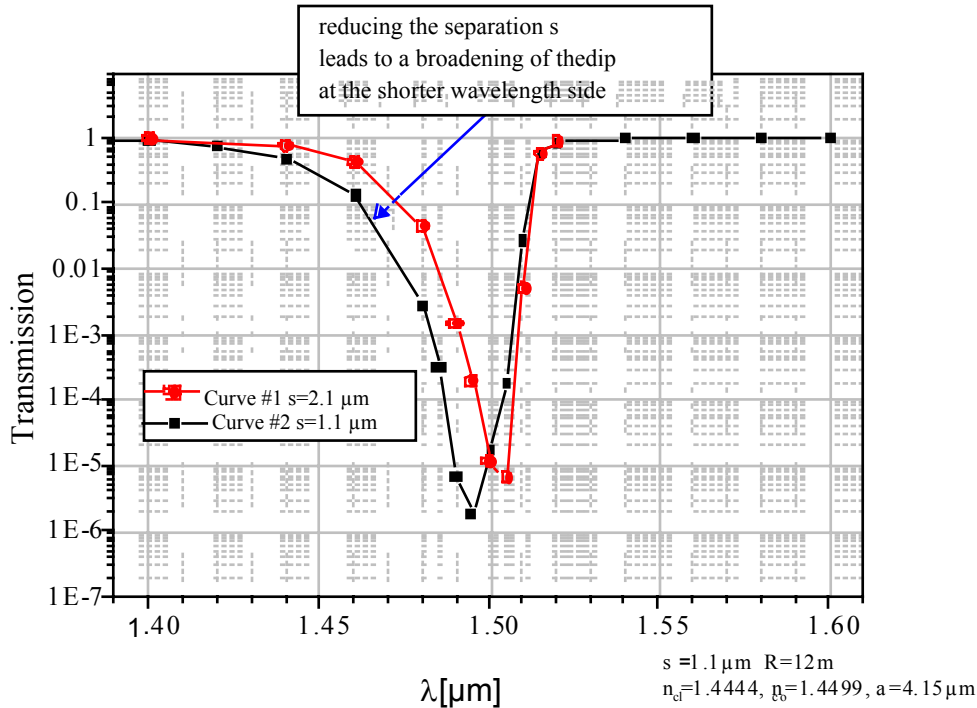


Figure 35 Cladding thickness dependence. The smaller the remaining cladding, the broader the dip. Total propagation length is 2 cm for these examples

This asymmetric behavior is due to the following: The modes in the polymer are not bound to the fiber but they extend into the slab. In this case, a large value of s is assumed so that a discussion in terms of the individual polymer modes is appropriate.

A simple 1-D picture, in which the polymer mode extends infinitely into the transverse direction, cannot be applied: additional modes, which are distinguished by their transverse order index, must be taken into account. The modal fields of Figure 30 and Figure 31 show that for the given boundaries, the mode in Figure 30 has a transverse order of 0 inside the polymer. The mode in Figure 31, however, has transverse order 2 inside the slab. Similarly, an infinite number of higher order modes exist, all of which have effective indexes slightly lower than the fundamental mode with transverse order 0. Therefore, the modes with which coupling can occur have effective indexes that are limited by the index of the fundamental mode on the high index side, but continuous towards lower indexes.

Consequently, a sharp drop in the transmission characteristics occurs when (approaching from the longer wavelength side) the slab mode with transverse index 1 is matched. Subsequently, the transmission rises slowly as decreasingly efficient coupling and loss to higher transverse order modes take place.

The other curves in Figure 35 show the influence of the remaining cladding thickness s on the dip shape. The smaller the value of s , the broader the dip. The reason is that, with decreasing separation between the fiber and the polymer slab, coupling to higher order transverse modes becomes more efficient which results in a broadening of the dip. The longer wavelength side is not influenced by this effect.

Amplitude modulation should be performed on the longer wavelength side of the dip, as there is a steeper slope than on the shorter wavelength side. The polishing depth for this application is not a crucial parameter. EO modulation efficiency can be 100% with a voltage on the order of 15 V which provides an electric field of 2-3V/ μm . The transmission is from 0.2 to 0.4, and the value $r_{33}=30\text{pm/V}$ is assumed.

3.6.2 Effect of Polymer Thickness and Refractive Index Variation

This section discusses the influence of polymer thickness and index on the transmission characteristics. The change of the dip position for a change of index ($\Delta n = 0.005$) and thickness ($\Delta d = 0.5\mu\text{m}$) is shown in Figure 36. This behavior can be estimated from simple 1-D analysis. The changes are in good agreement with the changes observed for the 1-D waveguide modes of the polymer. However, for smaller remaining cladding thickness, a careful 2-D analysis is necessary.

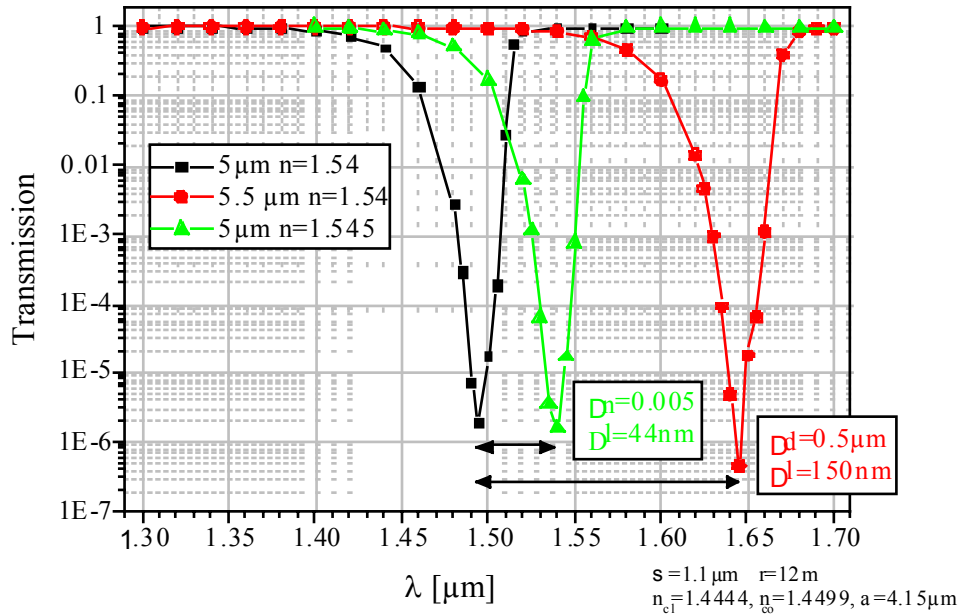


Figure 36 Influence of polymer thickness and index on the transmission behavior.

Chapter 4 Test Methodologies

This chapter reports the tests and results for static and dynamic WADMs modules, and describes the test methodologies developed for additional and final verification in the next phase of this project.

For static devices, only optical tests were performed. For dynamic devices, optical tests and optoelectronic/electrical tests were performed. The electrical investigations consisted of direct current (DC) and alternating current (AC) tests. Figure 37 shows the test setups.

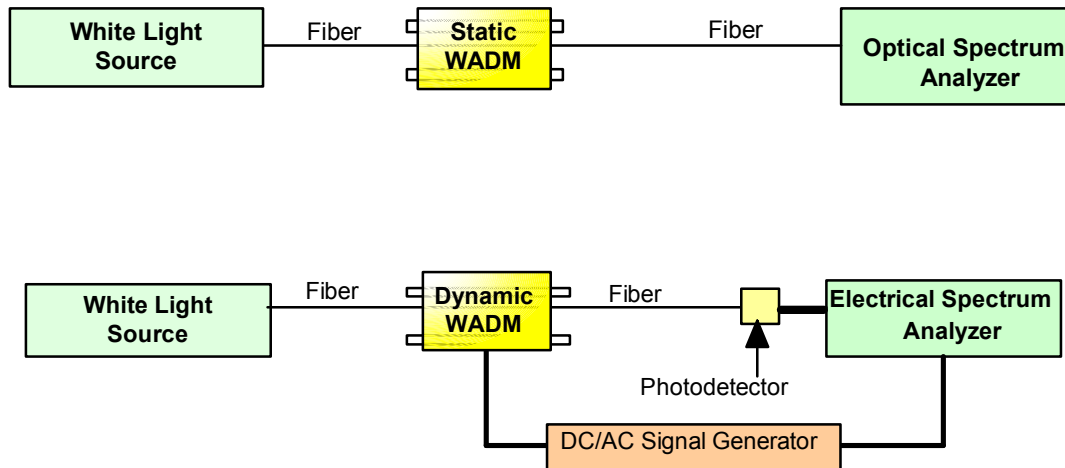


Figure 37 Test and Characterization Setups: Optical, Electrical

4.1 Optical Tests: Static and Dynamic Devices

This section describes the test methods and the objectives.

The static and dynamic WADMs were evaluated for spectral response characteristics. The HP70951B optical spectrum analyzer was used for measurements. The full spectral scattering matrix was obtained through the spectral response between each pair of the four ports. Note that the symmetry and reciprocity reduced the number of independent elements in the matrix.

Multiplexers and demultiplexers in DWDM systems are complex multi-passband filters. Through the input and output of a single fiber in an optical link, these devices combine and separate multiple wavelengths in and separate multiple wavelengths.

Key parameters, such as spectral shape and filtering characteristics, need testing. In particular, center wavelengths, bandwidth, insertion loss, and the ripple or flatness of each passband must be characterized. To ensure negligible crosstalk between the channels, test equipment must reveal high isolation between worst case adjacent and neighboring channels. It is also important to verify insertion loss uniformity among channels to evaluate the differential loss and the device ripple. If the multiplexers and the demultiplexers have upgrade ports to accommodate future capacity growth, it is recommended to perform similar tests on the upgrade passband. Such measurements are performed with an optical spectrum analyzer.

WADMs use various filtering technologies, such as dielectrics, acousto-optics, fiber gratings (IFOS design), arrayed waveguide gratings (AWGs), and others. Regardless of which filtering technologies are used, the principle function of the WADM is adding and dropping specific wavelengths, and allowing the remaining wavelengths to pass without degradation. Three routes need verification: in-out (pass-through or express), in-drop (drop) and add-out (add) paths. For each route, tests are performed to gauge

passband insertion loss (IL), ripple, channel isolation, optical return loss (ORL), and polarization dependent loss (PDL).

PDL, as a function of wavelength, can be verified by using a combination of a tunable laser and a polarization controller. Measuring ORL on all connectors is also essential, as high density WDMs typically contain multiple connector ports that increase the potential of high reflection. The values of ORL and PDL must be small in these devices. If not, high-bit-rate systems are adversely affected.

4.2 Preparation for Network Insertion Test

The primary goal of network insertion testing is performing a range of tests for insertion into next generation multi-wavelength communications, bit-parallel wavelength cluster computer networking, and sensor systems. The required preparation work for this effort was completed in this project. However, to complete this test plan, additional resources are necessary. It is expected to complete this task in the next Phase of this project.

Before deploying the WADM system in the field, certain parameters in a fiber plant must be characterized to assess which technology is appropriate for a fiber optic network. As line rates increase, the effects of chromatic dispersion and polarization mode dispersion (PMD) increase due to the distribution and the dispersion induced nonlinear effects. Following are descriptions of the necessary tests for this assessment.

The required dispersion can be determined by using chromatic dispersion analyzers to measure total dispersion in the fiber link. PMD analyzers gauge differential group delay (DGD). Optical time domain reflectrometers (OTDRs) characterize span loss (SL) and fiber length. The chromatic dispersion and PMD tests are usually not performed on newer fiber unless dispersion compensating devices (DCDs) are present in the system; these parameters are specified by fiber manufacturers. However, it is important to conduct such tests on old fiber plants that are considered for high bit rate transport such as OC-192 (10 Gbs), and for fiber distances great enough to strain the limitations of system dispersion.

Architecture interconnection tests corroborate the functionality and survivability of the networks' links which IFOS considers important. Optical network survivability is available exclusively over the electronic layer through SONET. These network systems are augmented by systems that allow static WADM functionality. Today's WADM systems are designed for point-to-point connectivity over long distances. It is expected that WDM systems will soon work in conjunction with dynamically reconfigurable WADMs.

Further testing has been determined necessary for the following reasons: service protection and essential aspects of the architecture are tested for network reliability, survivability and consistent service; high-performance switches and routers will route wavelength over complex networks; optical crossconnects and other advanced optical technologies will support flexible topologies; restoration architectures based on self-healing rings, diverse routing, or mesh-based distributed algorithms.

4.2.1 Communications Networks Test Plans

To fully evaluate the performance of the IFOS static and dynamic WADMs, systems level device testing will be undertaken by IFOS and partners. Currently, two dominant WADM technologies are employed: static WADMs based on composite fiber Bragg grating filters with optical circulators; arrayed waveguide grating (AWG) routers with wavelength independent switches. These current solutions require multiple discrete devices. Each device requires distinct fabrication methods, complicating the integration into one device. The size, the number of devices, of each node grows almost linearly with the number of wavelengths that can be dropped per node.

The IFOS device integrates the functionality of two discrete devices into one compact device at a significantly lower cost. In the next Phase of this project, IFOS will perform comparative testing of the IFOS optical WADM systems and the above mentioned technologies. Also, IFOS will provide experimental systems data comparing the three types of systems configured as complete WADM nodes.

Performance measures and network considerations on a systems level include the following: dispersion management, network scalability, link and channel capacity, reconfigurability, fault tolerance, and ease of network management. Experimental testing of the subsystems will be undertaken to yield data for evaluating the network considerations listed above. To support evaluation, the following systems level tests are in consideration.

4.2.1.1 High Bit Rate Amplified Link Bit Error Rate Measurements for WADM Nodes

This constitutes a set of measurements that implement an optically amplified, direct detection, on-off shift keying transceiver. The equipment considered for testing are the following: OC-12 (0.6228 Gbps), OC-48 (2.488 Gbps) and/or OC-192 (10 Gbps). Planned experimental data results include WADM receiver sensitivity, amplified spontaneous emission (ASE) suppression, and bit rate sensitivity penalty. Acquiring and interpreting this data will provide answers for the following network issues: dispersive behavior of filter (dispersion management) and frequency distortion introduced by filter (channel capacity). Figure 38 shows the test setup diagram to measure bit error rate (BER) for each WADM node.

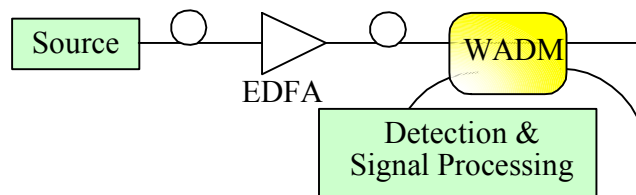


Figure 38 Setup for BER per WADM Node

Recirculating Loop BER Measurements

These measurements are derived by recirculating an optical stream through several passes of the WADM node. Obtaining experimental results will involve the following: channel equalization requirements; multiple insertion losses; cumulative dispersion effects due to the grating structures. Data interpretation will solve questions related to dispersion management requirements and network scalability. Figure 39 shows the test setup diagram to measure recirculating loop BER.

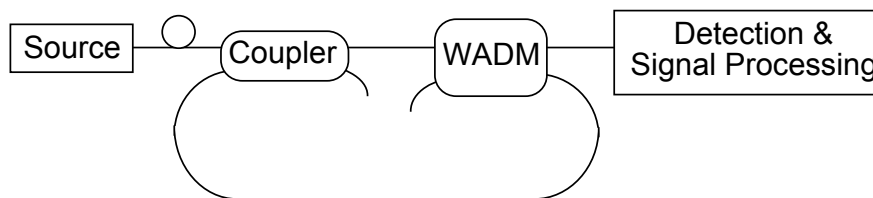


Figure 39 Setup for Recirculating Loop BER

Tuning Precision and Crosstalk Induced BER Penalty Measurements

These constitute a set of measurements of filter and source misalignments, spacing variations, and exploring tuning repeatability. The impact of misalignment is expected to have different associated penalties for each WADM architecture due to filter shape and demultiplexing properties. Test data will

provide information for the following: channel stability and channel registration requirements; coherent and incoherent channel interference; extinction ratios; channel suppression requirements. Data will be interpreted to solve answers to network scalability, link and channel capacity, reconfigurability, fault tolerance, and network management techniques. Figure 40 shows the test setup diagram to measure tuning precision and BER penalties induced by crosstalk.

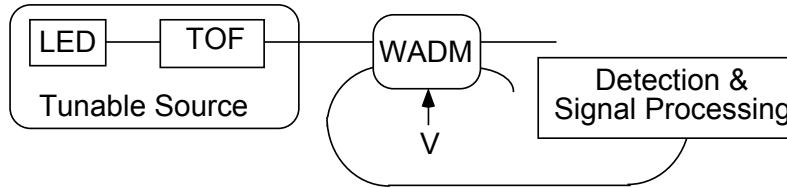


Figure 40 Setup for Tuning Precision and Crosstalk Induced Penalties

Device Characteristics and BER Penalty Measurements

The WADM node BER penalty due to device birefringence will be evaluated for operation in standard non-polarization maintaining fiber networks. BER penalties associated with tuning filter drift, and tuning and locking algorithms will be experimentally investigated for the three WADM node architectures. This data will be used to further infer the capabilities of each architecture with regard to network management techniques for tuning, locking, and network scalability. Figure 41 shows the test setup diagram to measure BER penalty due to device birefringence.

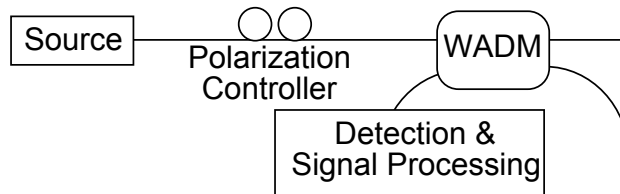


Figure 41 BER Penalty Measurement Setup

The experiments described above will be performed separately for the static and dynamic IFOS WADMs. The experiments that focus on tunability will be performed only with the dynamic IFOS device. In all cases, experimental results will also be used to modify the IFOS design, if found necessary, to improve crosstalk suppression and back reflection.

Chapter 5 Commercialization

This chapter discusses the marketing research and strategy for the wavelength add-drop multiplexer.

5.1 Market Potential

The proposed WADM access modules and spin-off filtering and switching products have significant market potential in multi-wavelength communications, long haul and short haul. Sensor systems, including demanding government programs in distributed dense optical computing such as bit-parallel computing, promises drastic increases in the information carrying capacity. No other known product has the combination of low-cost manufacturability, high-efficiency, high-speed, and compactness afforded by the proposed WADM devices.

This project has great potential to lead to a number of useful products including IFOS WADM access modules and spin-off filters, modulators, and switches. Such products have significant market potential in multi-wavelength communications, both long haul and short haul. The WADM business is characterized as a large and underserved market that is projected to grow to over \$7.2 billion by 2008.

5.2 Market Value

Currently, there appears to be no other optical WADM device that has the combination of properties possessed by the IFOS devices. These features, resulting from combining technologies used exclusively in the IFOS design, include the following:

- High resolution, ~ 0.1 nm
- Low insertion loss, < 0.2 dB for static WADMs, < 1 dB for dynamic WADMs
- Low crosstalk, < -30 dB
- Light weight and compact size
- Low cost, $\sim \$200$ for static WADMs, $\sim \$400$ for dynamic WADMs

In dynamic devices, the following features are also included:

- High tunability speed, ~ 1 nanosecond for the full spectral range
- Low voltage requirements, < 15 V

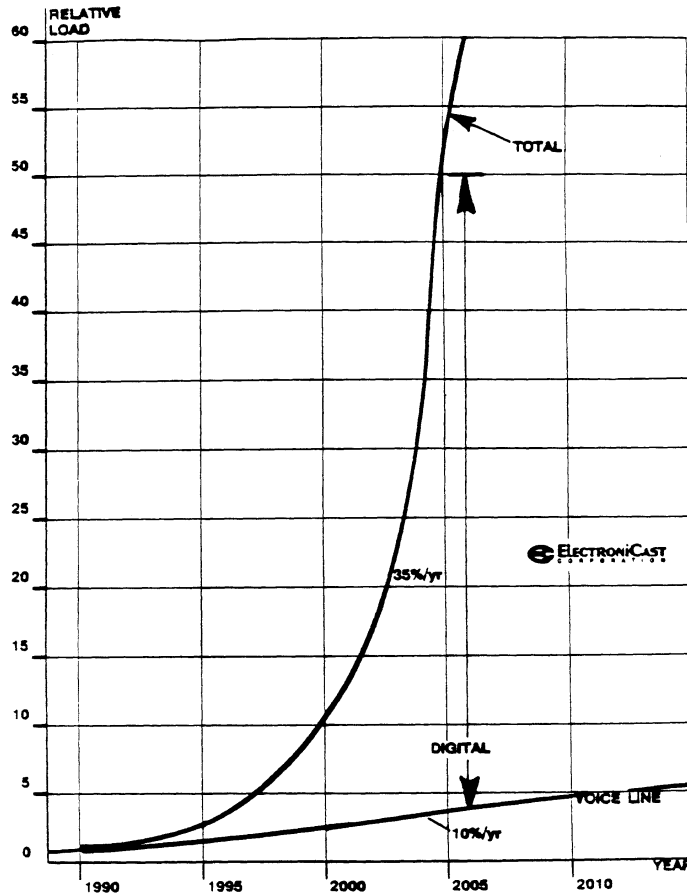


Figure 42 Telecommunication Network Bandwidth Trend

Figure 42 illustrates the Telecommunication Network Bandwidth Trend [16]. This trend is based on the implementation of digital transport of telecommunications services. The transmission of digital signals is forecast to boost the growth of telecommunications network bandwidth by 35% per year from 1996 to 2006, compared with 10% per year for analog voice lines [16]. The wavelength filtering and switching technology developed in this project is applicable to a wide range of fiber components including WADMs, filters and switches. The global market for WADMs is predicted to reach \$7.2 billion worldwide. The maximum throughput per fiber for networks, based on these WADMs, is predicted to reach 10 Tbps by 2008. Refer to Figure 43. IFOS is developing such WADM components and it is exploring systems that make intensive use of these components.

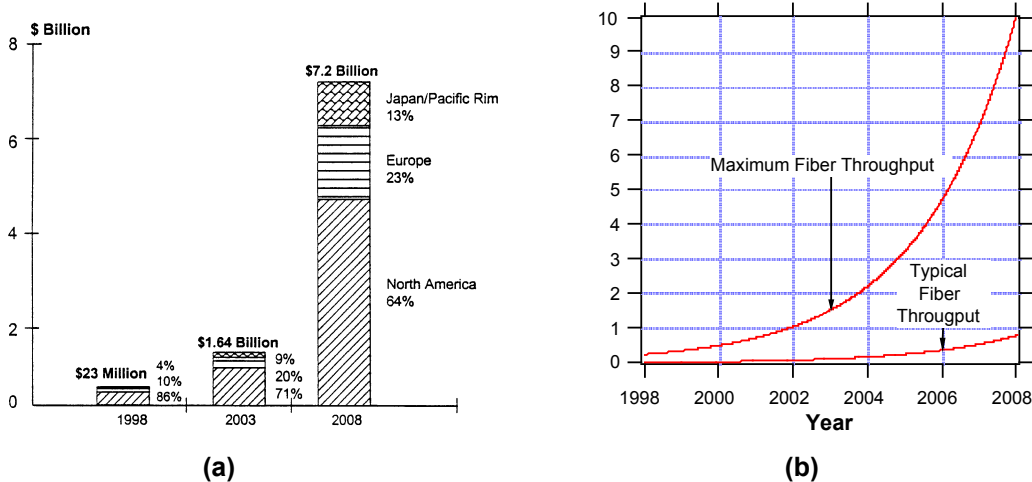


Figure 43 WADM Trends

- (a) Global consumption value trends of WADMs by region
- (b) WADM throughput trends: the maximum throughput in 2008 assumes 256 channels at 40 Gbps [16]

Low cost, high volume production of photonic components and systems is of vital importance for the U.S.A. to achieve the proliferation of Fiber-To-The-Home (FTTH) or Fiber-To-The-Desk (FTTD), independent of foreign suppliers for optoelectronic components. In line with this demand, the cost of optical transmitters has been rapidly dropping. Refer to Figure 44. As seen, the unit cost of an OC-192 (10 Gbps) transmitter is projected to drop from the present value of several thousand dollars to less than \$100 by 2008. OC-12 (51 Mbps) and OC-3 (155 Mbps) transmitters are already near or under \$100 per unit.

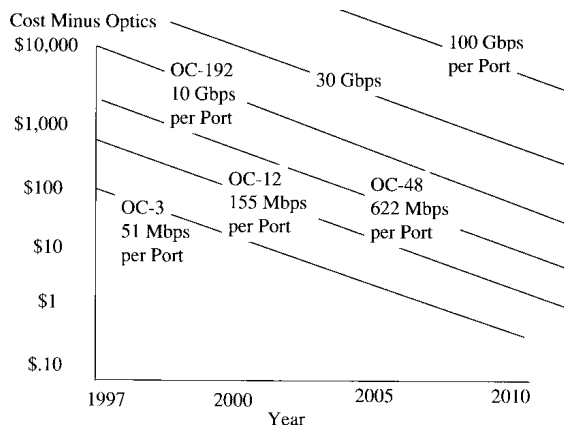


Figure 44 Cost Minus Optics for Optical Communications

The advantages of WDM provide enhanced capacity, as well as more reliable and less costly systems than the equivalent electronic systems. Where WDM can be cost justified, it is now being seriously deployed. Such a cost justification occurs mostly in long-distance networks where annual budgets for transmission equipment are very large. However, while a top-of-the-line 16-wavelength transmission system costs a couple of million dollars to deploy for each point-to-point segment, long distance carriers can quickly recapture the cost with the additional bandwidth the systems supply.

A comparable financial outlay for faster Time-Division Multiplexed (TDM)-based Synchronous Optical

NETwork (SONET) gear would yield significantly less bandwidth. WDM in the enterprise environment is still an unproven concept mainly due to implementation cost and its future depends on both technological and economic questions. On the technology side, there are the issues of whether WDM can be scaled down in a manner that is appropriate to enterprise networking requirements (www.cir-inc.com).

There is also the issue of whether WDM can be used to do more than just supply large bandwidth for the telecommunications backbone. However, it can be shown that for channel extension applications among corporate data centers, WDM systems already make sense. For example, experimental LANs have been built in the laboratory that allow users to access the network by tuning to a certain wavelength using WDM (www.cir-inc.com).

5.3 WADM Applications

IFOS believes its WADMs will stimulate many advanced fiber-optic system implementations in communications, computer networking, sensor systems, and fiber-optic based spectroscopy. The highly efficient static and high-speed dynamic IFOS WADMs enable the lower-cost build-out of high-bandwidth optical networks by providing efficient and dynamic wavelength routing and switching capabilities. Potential applications of the IFOS static and dynamic WADMs include the following:

- Dense wavelength division multiplexed (DWDM), long haul and short haul telecommunications
- Dynamic wavelength routing and network reconfiguration
- Dynamic wavelength-selective receivers
- DWDM nodes with static WADM for control and dynamic WADMs for data
- Dense optical computing including bit-parallel wavelength computer networking
- Wavelength division multiplexed sensors
- Spectroscopy involving wavelength selection from a continuous spectrum

The application areas of initial focus include Next Generation Networks, the Next Generation Internet, bit parallel wavelength, optical cluster computer networking, and sensor arrays. To further the goal of commercialization, IFOS continues collaboration with many industry and technical leaders, including the Mathematical, Information and Computational Sciences Division of the Department of Energy, Optical Coating Laboratories, Inc., Oak Ridge National Laboratory, California Institute of Technology's Jet Propulsion Laboratory, Cisco, Uniphase, and Lawrence Livermore National Laboratory.

The following sections describe two potential applications: Bit Parallel Wavelength Cluster Computer Networking and Sensor Networks

5.3.1 Bit Parallel Wavelength Cluster Computer Networking

IFOS has explored the applications of its technology to bit parallel wavelength (BPW) cluster computer networking developed by Bergman et al [14], [15] at the California Institute of Technology's Jet Propulsion Laboratory. For this project, the Principal Investigator and the staff of IFOS had several meetings with Dr. Bergman's team at the Jet Propulsion Laboratory.

BPW optical linking is an interconnect and local area network transmission concept for computer communications based on spectrally encoding one or more computer words into a wavelength datagram. At the physical and data link level, this system resembles an optical ribbon cable, except that all the bits pass on one fiber optic waveguide. At the network level, such fiber optic link segments can be optically interconnected. To do so requires using 2x2 optical switches into ShuffleNet or other architectures that permit a photonic packet to pass from source to destination without encumbrance from the extra delay and the bandlimiting associated with electronic switching and regeneration. Unique properties of such a system include low latency (< 10 ns), very high bandwidth (> 100Gbps per port), precise time alignment (< 10 ps) of the individual word bits over km distances, and dynamic scalability to support cluster

computing and distributed supercomputing.

Novel system elements include the following: BPW fiber-optic link that uniquely maintains wavelength channel time alignment; an innovative parallel stepped-wavelength channel optical transmitter that time synchronizes each laser diode element at its optical output; a spectral encoder/decoder that adds fault tolerance and optical message addressing capability; a special multi-wavelength technique for transmitting and maintaining time aligned ultra-short pulses as parallel bits through fiber-optic media. Applications include teraflop high performance parallel computing and input output (IO) bound computing problems.

5.3.2 Sensor Networks

IFOS has developed a grating based sensor array for National Aeronautics and Space Administration in which multiple distributed sensor gratings operate by reflecting signals in different wavelength bands. Presently, static demultiplexing is used. For the next Phase, a possible task is demonstrating an application of the WADM: obtain a dynamic, reconfigurable sensor array. To do so, IFOS is considering incorporating dynamic WADMs, that were developed under this project, in this sensor system to dynamically demultiplex the multi-wavelength signal. This would be achieved by tuning into the wavelength band occupied by the sensor chosen for interrogation. When sensor measurand information is contained in the wavelength domain, dynamic tuning will allow determining the wavelength and the measurand. To track the wavelength of one channel at a time, a 2-port device (in either notch or bandpass configurations) will suffice. Concatenated static WADMs will also be considered for simultaneous multiwavelength demultiplexing.

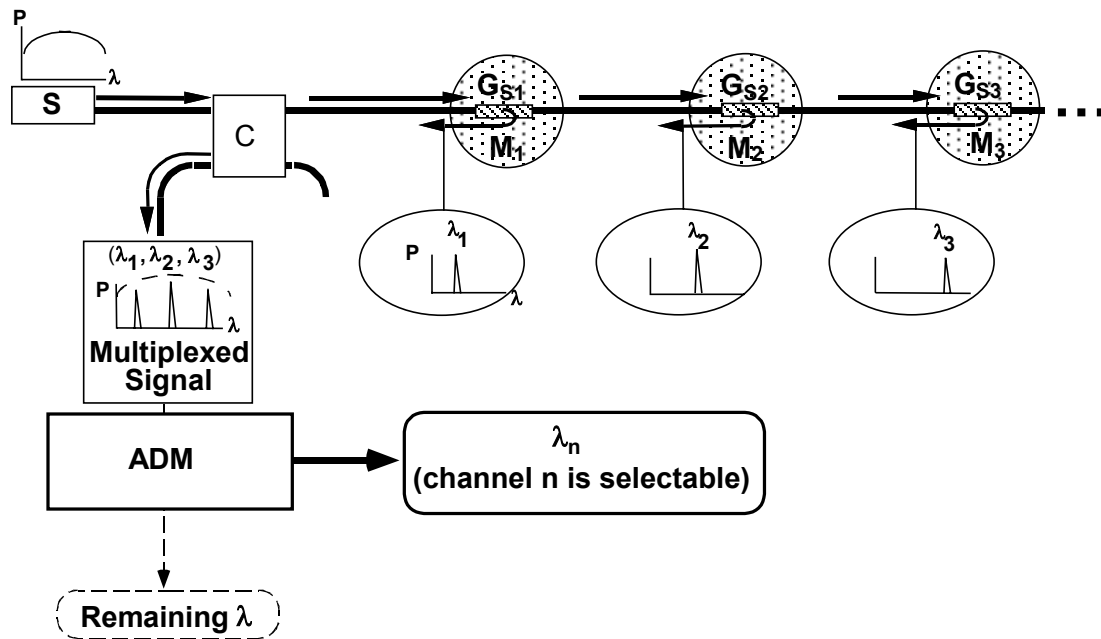


Figure 45 IFOS WDM Sensor System

Figure 45 illustrates the IFOS WDM sensor system design concept using fiber Bragg grating sensors, GS_n , and a dynamic WADM for demultiplexing. Illuminated by broadband source, S, sensor grating GS_n , attached to active or transducer materials M_n , reflects at wavelengths λ_n . λ_n is the network address of sensor GS_n . WDM allows transparency of each grating to the signals reflected by the other gratings. The coupler C taps out the reflected signals. The WADM then selects the channel of interest. For a 2-port wavelength-selective switch, one channel at a time is selected and the remaining wavelengths are

discarded. For the 4-port WADMs the remaining wavelengths can be kept for further processing as may be required by some specialized applications.

5.4 Commercial Expansion

During this project for photonic add-drop multiplexers, interaction with potential customers has generated the concept of a *hitless OADM*, in which no data down time is introduced during channel tuning/switching. IFOS has developed a paper concept for a modified version of the tunable OADM that was developed in this program. Advanced packaging, MEMS-like switching, and optical power control modules (OPCMs) complete with electronics, are being designed as a result of Phase II of this program. This, and the results of other IFOS programs, will be the subject of future proposals.

IFOS is presently fabricating and testing WADMs based on side-polished fibers with long interaction length. For test and fabrication, the IFOS facilities have been upgraded by, for example, installing three portable class 100 clean rooms, HEPA sub micron particle filters, and floor entrance sticky tabs. In addition the complete lab area outside the three clean rooms was upgraded to class 1000 through the use of air filters and floor entrance tabs.

Chapter 6 Conclusion

In this Project, based on the objectives of Phase II proposal, the traffic-grooming problems for WDM/SONET ring network were studied. This part of the work consists of two parts.

In the first part of the work, the single ring case was considered. IFOS is the first to provide formal mathematical problem specifications on some variations of the WDM/SONET ring architecture. The problems turn out to be integer linear programming (ILP) problems. Due to the nature of the problems, solving the ILPs directly with exhaustive search methods was not practical for current computational capabilities. Hence, two heuristics were proposed to find the near-optimal solutions for different network architectures. One random search heuristic, which is based on “simulated annealing” algorithm, has reached the best networking savings in its class so far, to the best of our knowledge. It was also concluded that the multi-hop approach will usually achieve better ADM savings when the grooming ratio is large, however, it consumes more wavelengths.

In the second part of the study, some preliminary work on traffic grooming in interconnected ring networks was completed. Three strategies are proposed for interconnecting double rings. For each interconnection strategy, the problem is successfully broken down into several independent small problems each on a single ring network. Although the small problems can be solved by the heuristics proposed in the first part of the study as well, the heuristics are usually inefficient when they are applied to some of the rings because these rings inherently have very special traffic patterns. Two new heuristics are proposed and the three interconnection strategies are compared in terms of the network cost. Also, some new results on traffic grooming on interconnected multi-ring networks are provided.

In the design and simulation portion of this project, the static and dynamic WADM design heuristics are established. This is accomplished by studying precursors to the WADM device as well as the WADM itself. This method permits us to learn about the WADM by studying simpler building blocks which are both more easily modeled as well as more easily fabricated. In fact, these full couplers, switches, and attenuators are very interesting devices in their own rights, both from a design standpoint, as well as a commercial standpoint. Through this work, optimized design parameters are established for the WADM, as are fabrication tolerances for these various parameters.

Much was learned through this project about the design WADMs and their deployment in optical networks. Although development work in several areas remains to be done before these devices and networks are fully deployed in the marketplace, great strides were made towards that goal.

Chapter 7 References

- [1] Telcordia GR-2918-CORE, Issue 3, March 1999, "Dense Wavelength Division Multiplexing Systems with Digital Tributaries for use in Metropolitan Area Applications: Common Physical Layer Generic Criteria"
- [2] ITU-T Recommendation G.692, "Optical Interfaces for Multichannel Systems with Optical Amplifiers", October 1998
- [3] ITU-T Recommendation G.959.1, "Optical Transport Network Physical Layer Interfaces", February 2001
- [4] Telcordia GR-1312-CORE, Issue 3, April 1999, "Generic Requirements for Optical Fiber Amplifiers and Proprietary Dense-Wavelength Division Multiplexed Systems"
- [5] ITU-T Recommendation G.709, "Interfaces for the Optical transport Network (OTN)", February 2001
- [6] Draft ITU-T Recommendation G.798, "Characteristics of Optical Transport Networks (OTN) Hierarchy Equipment Functional Blocks", February 2001
- [7] Gerstel, O., P. Lin, and G. Sasaki. Wavelength Assignment in WDM ring to minimize cost of embedded SONET rings. in Proc., IEEE INFOCOM '98. March 1998. San Francisco, CA
- [8] Gerstel and Sasaki, Cost effective traffic grooming in WDM rings. Proc. IEEE INFOCOM '98, March 1998: p. 69-77.
- [9] Modiano, E.H. and A.L. Chiu, Traffic grooming algorithms for minimizing electronic multiplexing costs in unidirectional SONET/WDM ring network. Proc., CISS '98, March 1998.
- [10] Simmons, J.M., E.L. Goldstein, and A.A.M. Saleh, Quantifying the benefit of wavelength add-drop in drop WDM rings with distance-independent and dependent traffic. IEEE/OSA Journal of Lightwave Technology, 1999. 17: p. 48-57.
- [11] G. Zhang, X. and C. Qiao, An Effective and Comprehensive Solution for Traffic Grooming and Wavelength Assignment in SONET/WDM Rings. Proc. SPIE, 1999. 3531: p. 221-232.
- [12] Wang, J., et al., Improved approaches for cost-effective traffic grooming in WDM ring networks: non-uniform traffic and bidirectional ring. IEEE ICC 2000, 2000.
- [13] Laarhoven, P.J.M.v., Theoretical and Computational Aspects of Simulated Annealing, Centre for Mathematics and Computer Science. 1988.
- [14] LA Bergman, AJ Mendez, LS Lome, 'Bit-parallel wavelength links for high performance computer networks', *SPIE Critical Review*, CR62, 210, 1996.
- [15] LA Bergman, 'Future directions in all-optical networks', in *Proc. DoD Fiber Opt. & Photonics Conf.*, McLean, Virginia (March 22-24), 1994, 109-12.
- [16] ElectroniCast, 'Dense WDM/Optical Amplifier Market & Technology Overview', in San Jose, CA, 1998.